Supporting Information

Multishelled Si@Cu Microparticles Supported on 3D Cu Current Collectors for Stable and Binder-free Anodes of Lithium-ion Batteries

Zailei Zhang,[†,‡,‖] Zhong Lin Wang[*,†,‡,‖,§] and Xianmao Lu[*,†,‡,‖]

[†] *Beijing Institute of Nanoenergy and Nanosystems, Chinese Academy of Sciences, Beijing 100083, China.*
[‡] *School of Nanoscience and Technology, University of Chinese Academy of Sciences, Beijing 100049, China.*
[‖] *CAS Center for Excellence in Nanoscience, National Center for Nanoscience and Technology (NCNST), Beijing, 100190, China.*
[§] *School of Materials Science and Engineering, Georgia Institute of Technology, Atlanta, GA 30332–0245, USA.*
**Correspondence authors. emails: zlwang@gatech.edu and luxianmao@binn.cas.cn.*

METHODS

Synthesis of 3D Cu@Al_2O_3 Core-shell Nanowires. Trimethyl aluminum and H_2O were used as precursors to deposit Al_2O_3 on 3D Cu nanowires at 200 ^oC at a deposition rate of about 1 nm per cycle to form a 50-nm thick Al_2O_3 layer using an atomic layer deposition (ALD) equipment (PICOSUN/SUNALE R-200, Finland).

Synthesis of 3D Cu@TiO_2 Core-shell Nanowires. Titanium tetrachloride and H_2O were used as precursors to deposit TiO_2 on 3D Cu nanowires at 200 ^oC at a deposition rate of about 1 nm per cycle to form a 50-nm thick TiO_2 layer *via* ALD.

Synthesis of 3D Cu@HfO_2 Core-shell Nanowires. Tetrakis(dimethylamido) hafnium(IV) and H_2O were used as precursors to deposit HfO_2 on 3D Cu nanowires at 200 ^oC at a deposition rate of about 1 nm per cycle to form a 50-nm thickness HfO_2 layer *via* ALD. The tetrakis(dimethylamido) hafnium(IV) precursor was kept at 80 ^oC during deposition.

Synthesis of 3D Cu@Al Core-shell Nanowires. The as-prepared 3D Cu nanowires on Cu foil were coating with Al using magnetron sputtering. The base pressure of the chamber was below 1×10^{-6} Torr. The deposition power was 100 W and the deposition time was 30 min.

Preparation of $Cu(OH)_2$@Au Core-shell Nanowires by Thermal Evaporation and 3D Cu@Au Nanowires by H_2 Reduction. The as-prepared $Cu(OH)_2$ nanowires on Cu foil were loaded into a Denton ultra-high vacuum electron beam evaporation coating machine (Denton Vacuum/Explore 14) for thermal evaporation of Au on the surface of $Cu(OH)_2$ nanowires. In the processes of thermal evaporation, the power was 90 W and the deposition time was 0.5 h. The resulting samples of $Cu(OH)_2$@Au core-shell nanowires on Cu foil were placed in a tube furnace and treated under Ar/H_2 at 350 ^oC for 1 h (ramping rate of 5 ^oC min^{-1}) to obtain 3D Cu@Au.

Figures

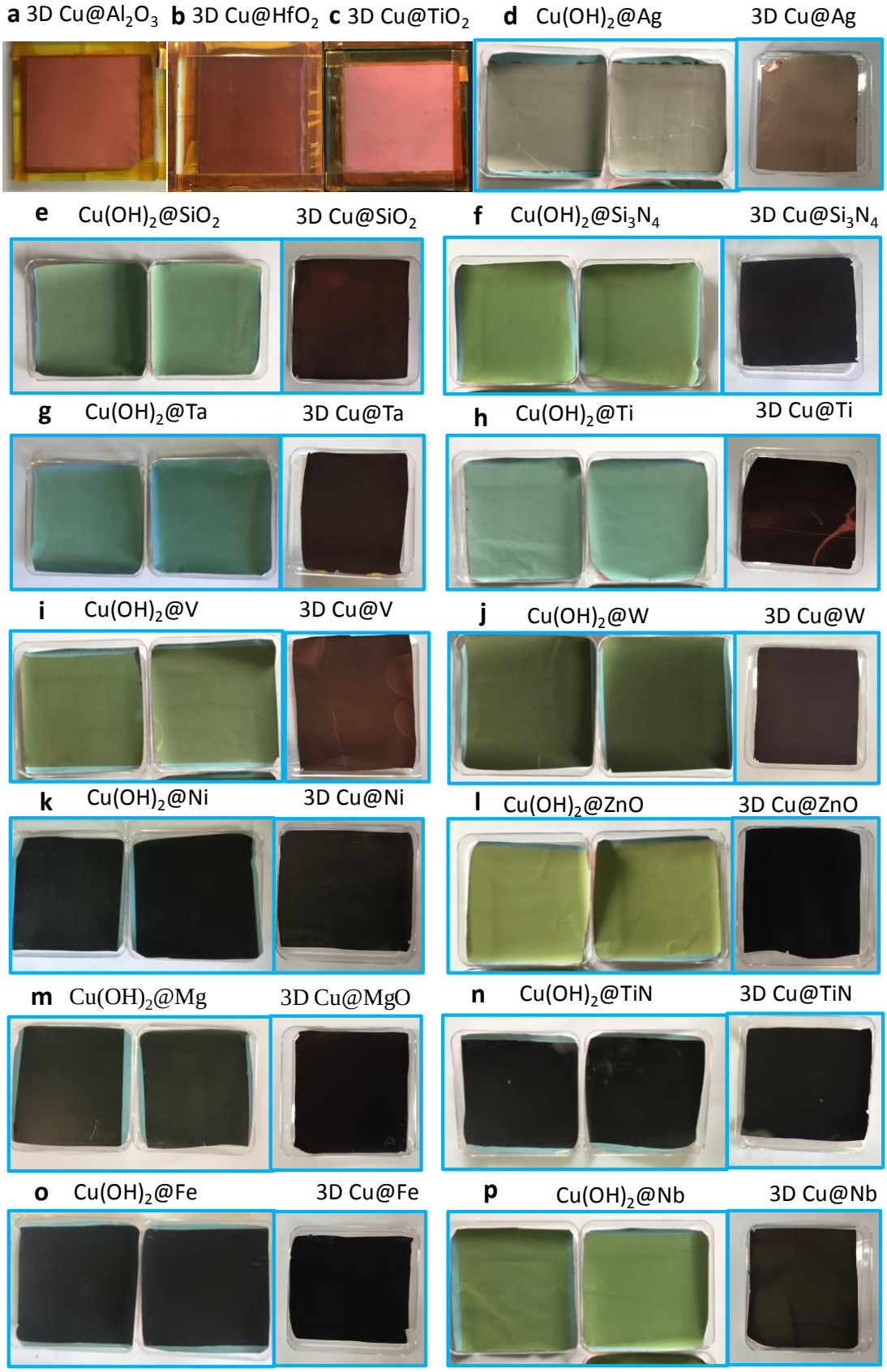

Figure S1. Photographs of **(a)** 3D Cu@Al_2O_3. **(b)** 3D Cu@HfO_2. **(c)** 3D Cu@TiO_2. **(d)** $Cu(OH)_2$@Ag

and 3D Cu@Ag. **(e)** $Cu(OH)_2$@SiO_2 and 3D Cu@SiO_2. **(f)** $Cu(OH)_2$@Si_3N_4 and 3D Cu@Si_3N_4. **(g)** $Cu(OH)_2$@Ta and 3D Cu@Ta. **(h)** $Cu(OH)_2$@Ti and 3D Cu@Ti. **(i)** $Cu(OH)_2$@V and 3D Cu@V. **(j)** $Cu(OH)_2$@W and 3D Cu@W. **(k)** $Cu(OH)_2$@Ni and 3D Cu@Ni. **(l)** $Cu(OH)_2$@ZnO and 3D Cu@ZnO. **(m)** $Cu(OH)_2$@Mg and 3D Cu@MgO. **(n)** $Cu(OH)_2$@TiN and 3D Cu@TiN. **(o)** $Cu(OH)_2$@Fe and 3D Cu@Fe. (**p)** $Cu(OH)_2$@Nb and 3D Cu@Nb. **Note:** Each square is 10 cm x 10 cm.

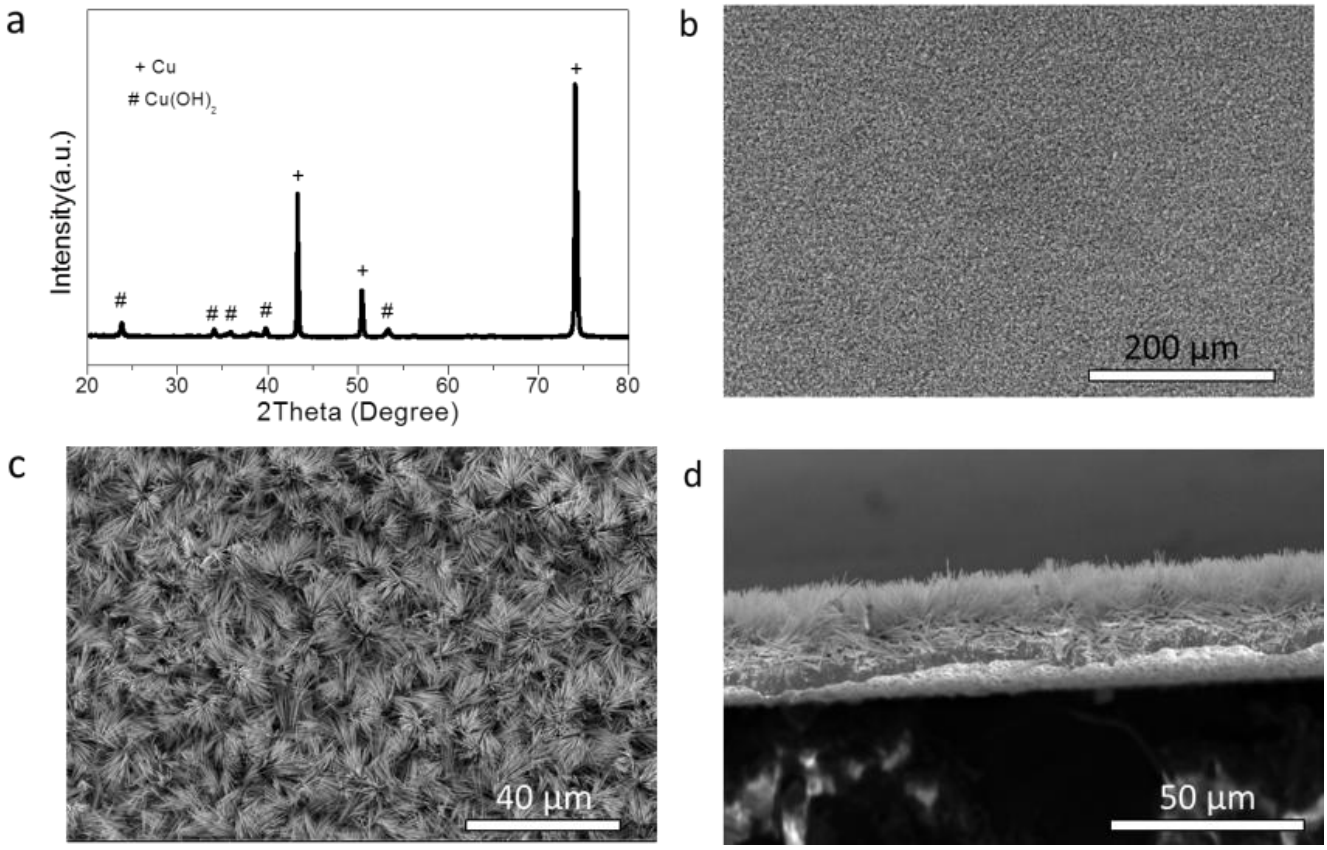

Figure S2. (a) XRD pattern. (**b,c)** Top-view SEM images. (**d)** Cross-sectional SEM image of $Cu(OH)_2$ nanowires.[1]

The XRD pattern of the $Cu(OH)_2$ nanowires coated on Cu foil confirm the sample is composed of $Cu(OH)_2$ (PDF no. 96-900-78503) and Cu (PDF no. 96-710-1265).

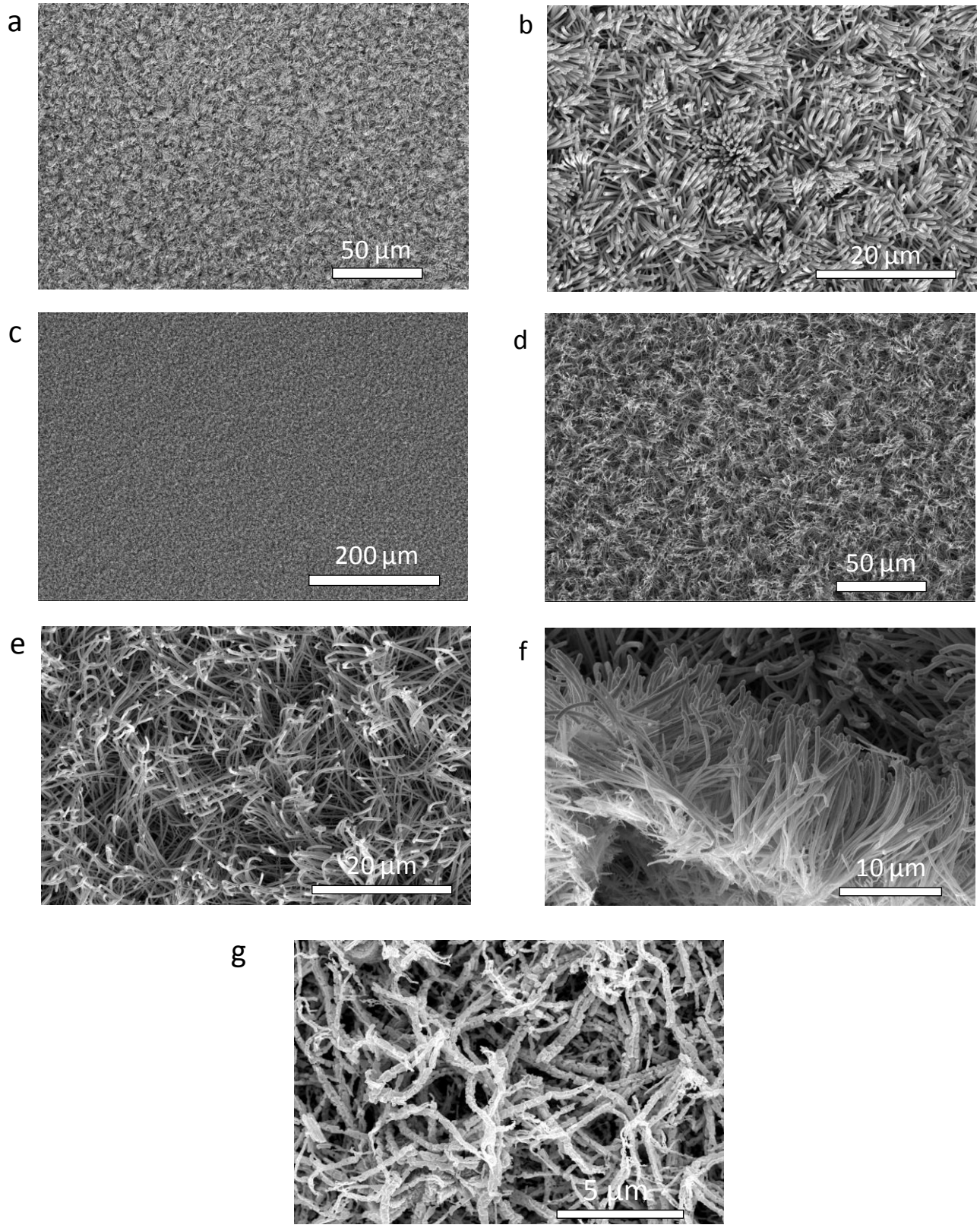

Figure S3. SEM images of **(a,b)** $Cu(OH)_2$@Cu nanowires. **(c,d,e)** Top view 3D Cu nanowires. **(f)** Cross-sectional of 3D Cu nanowires. **(g)** Kinked Cu nanowires formed by reducing $Cu(OH)_2$ nanowires.

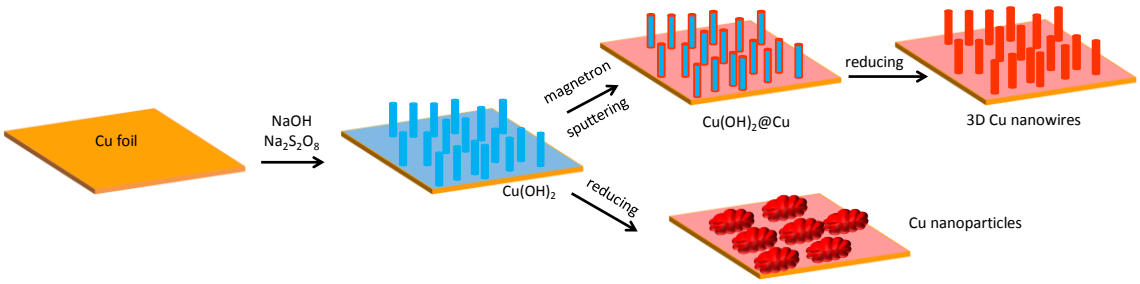

Schematic illustration S1. Schematic illustration for the formation of (top) 3D Cu nanowires by magnetron sputtering a Cu protection layer on $Cu(OH)_2$ nanowires followed by H_2-reduction and (bottom) kinked Cu wires and Cu nanoparticles formed by reducing $Cu(OH)_2$ nanowires without the Cu protection layer.

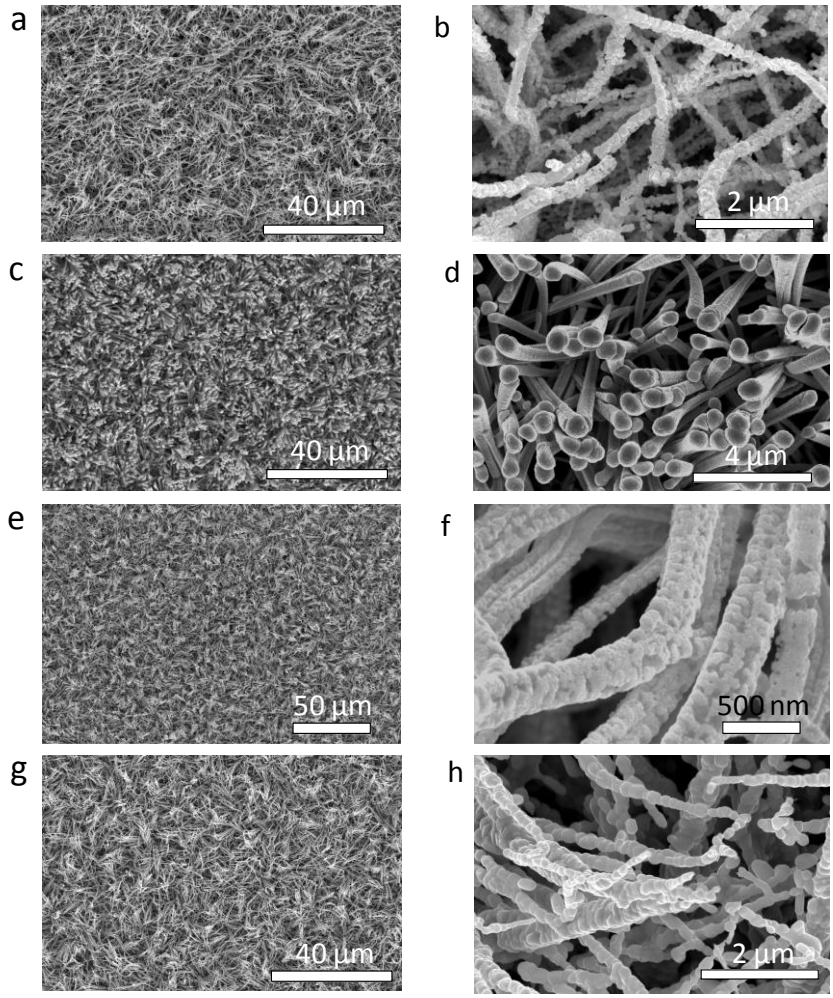

Figure S4. SEM images of **(a,b)** Magnetron sputtering at 100 W for 0.5 h and H_2-reduction at 300 ^oC for 1 h. **(c,d)** Magnetron sputtering at 200 w for 1 h and H_2-reduction at 300 ^oC for 1 h. **(e,f)** Magnetron sputtering at 100 W for 1 h and H_2-reduction at 400 ^oC for 2 h. **(g,h)** Magnetron sputtering at 100 W for 1 h and H_2-reduction at 600 ^oC for 1 h.

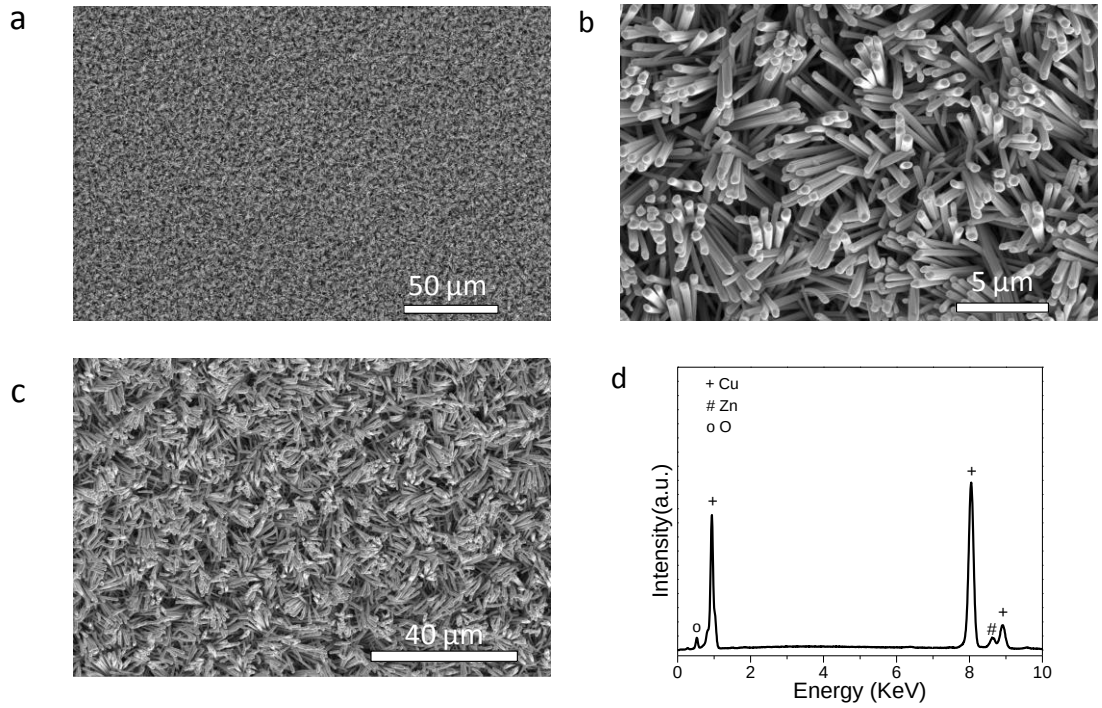

Figure S5. (a,b) SEM images of $Cu(OH)_2$@ZnO nanowires. **(c)** SEM image and **(d)** EDS analysis of 3D Cu@ZnO nanowires.

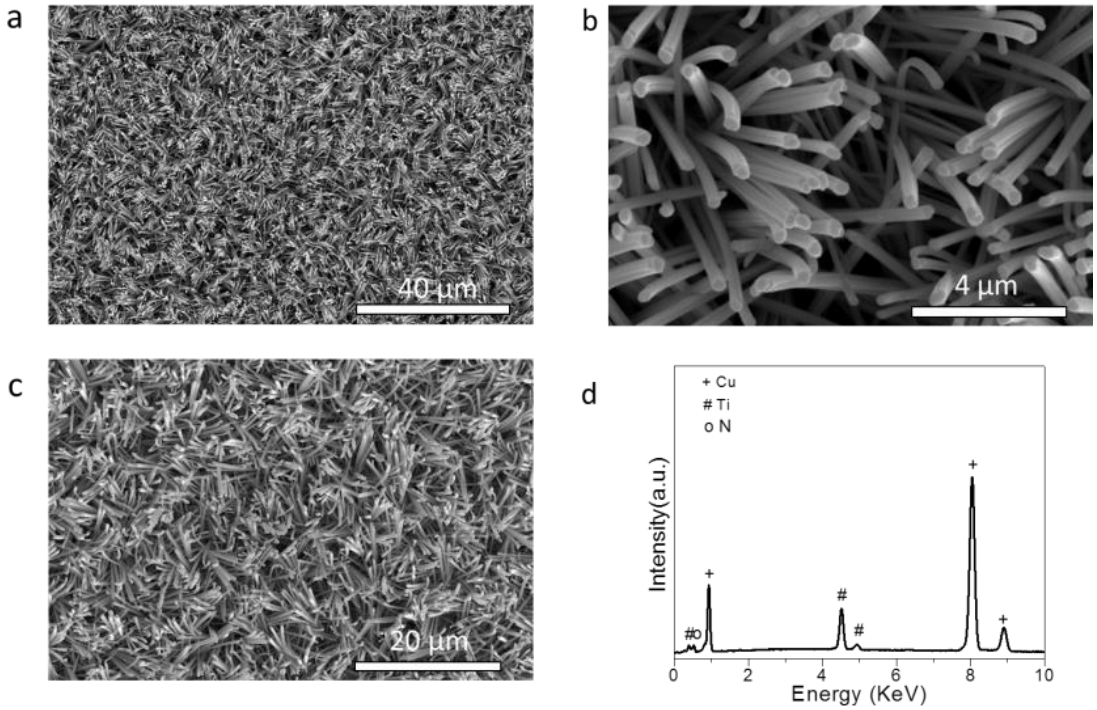

Figure S6. (a,b) SEM images of $Cu(OH)_2$@TiN nanowires. **(c)** SEM image and **(d)** EDS analysis of 3D Cu@TiN nanowires.

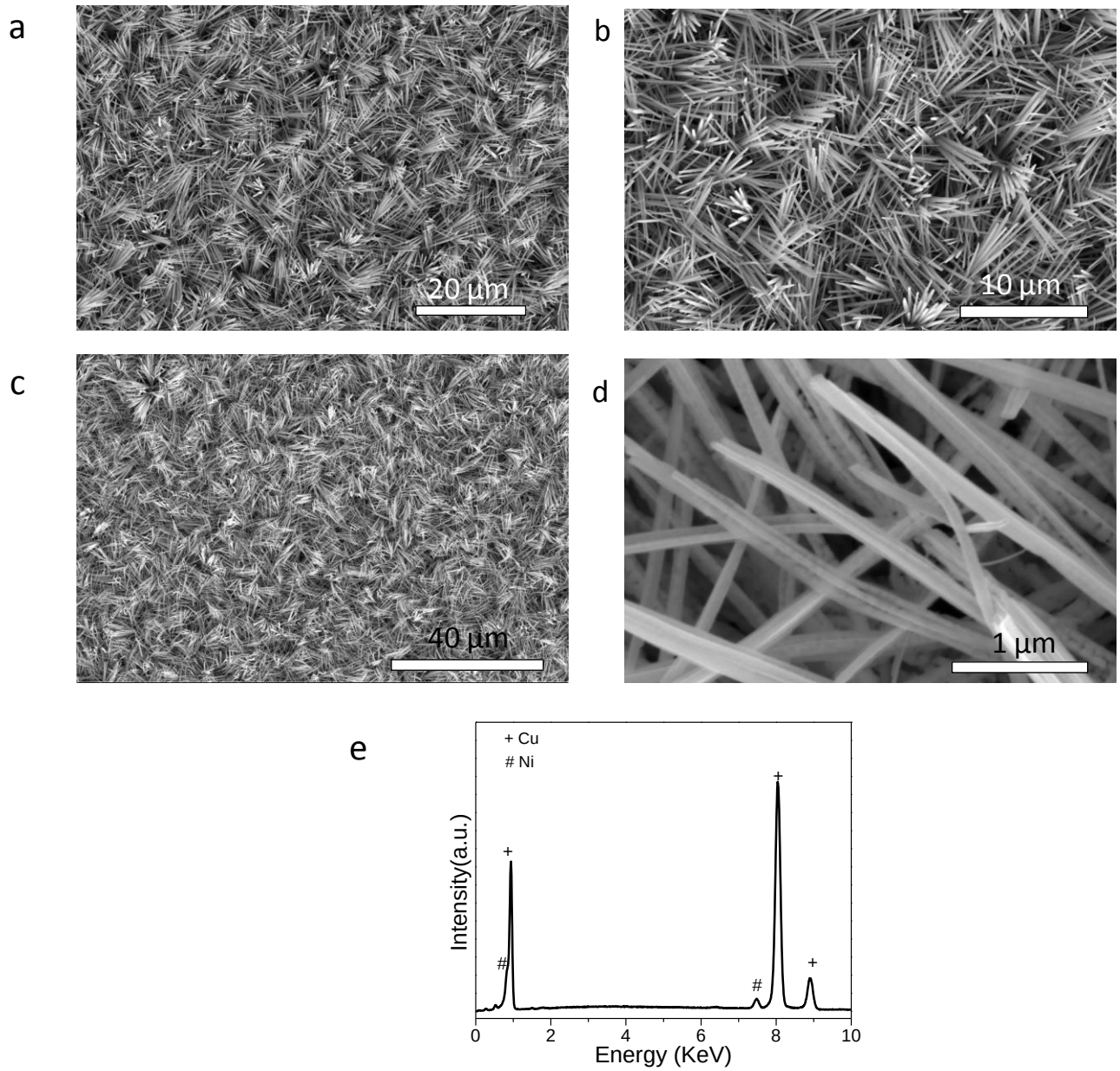

Figure S7. (a,b) SEM images of $Cu(OH)_2$@Ni nanowires. **(c,d)** SEM images and **(e)** EDS analysis of 3D Cu@Ni nanowires.

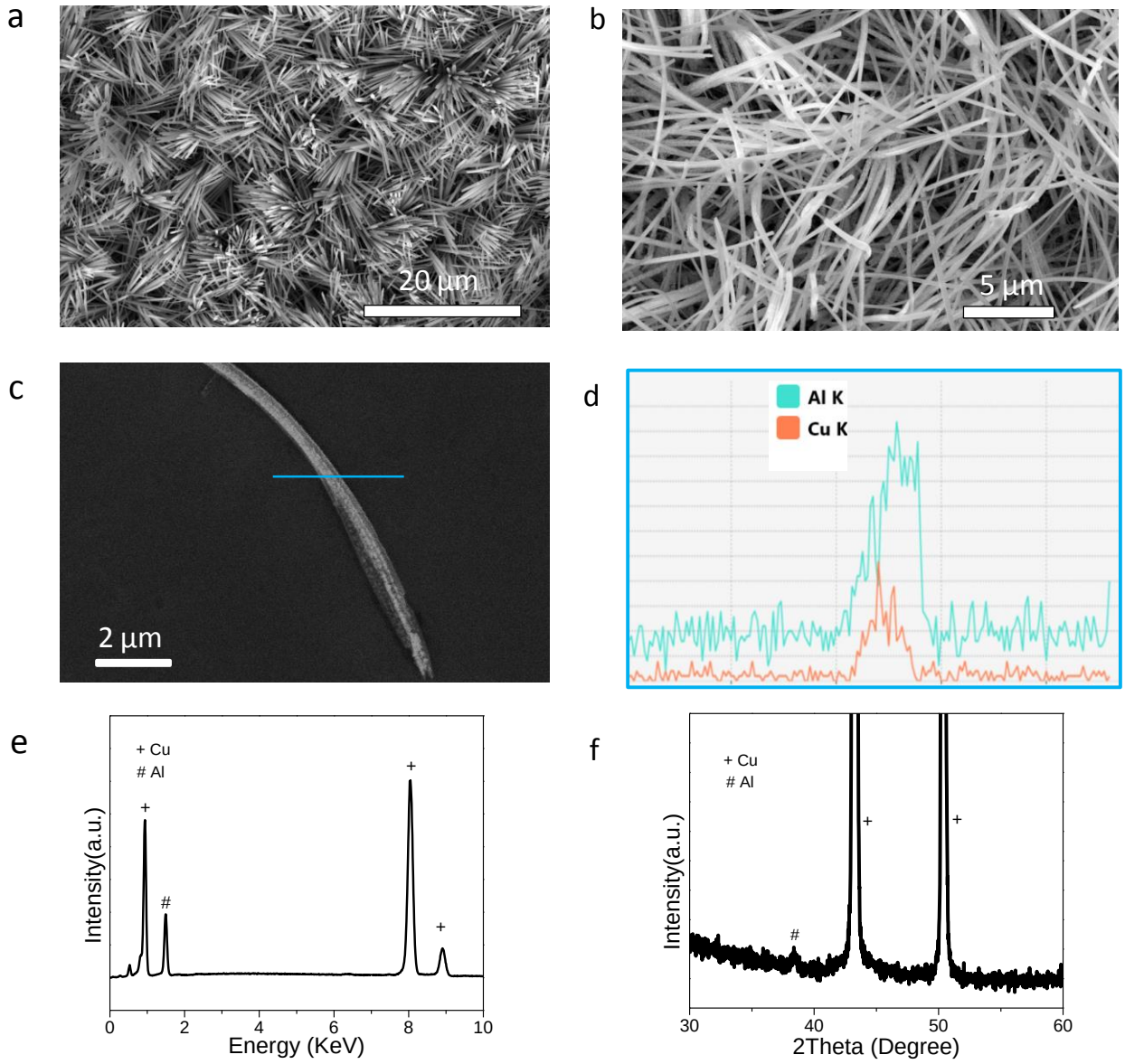

Figure S8. (a) SEM image of $Cu(OH)_2$@Al nanowires. **(b,c)** SEM images, **(d)** EDS line-scan profiles, **(e)** EDS spectrum, and **(f)** XRD pattern of 3D Cu@Al nanowires.

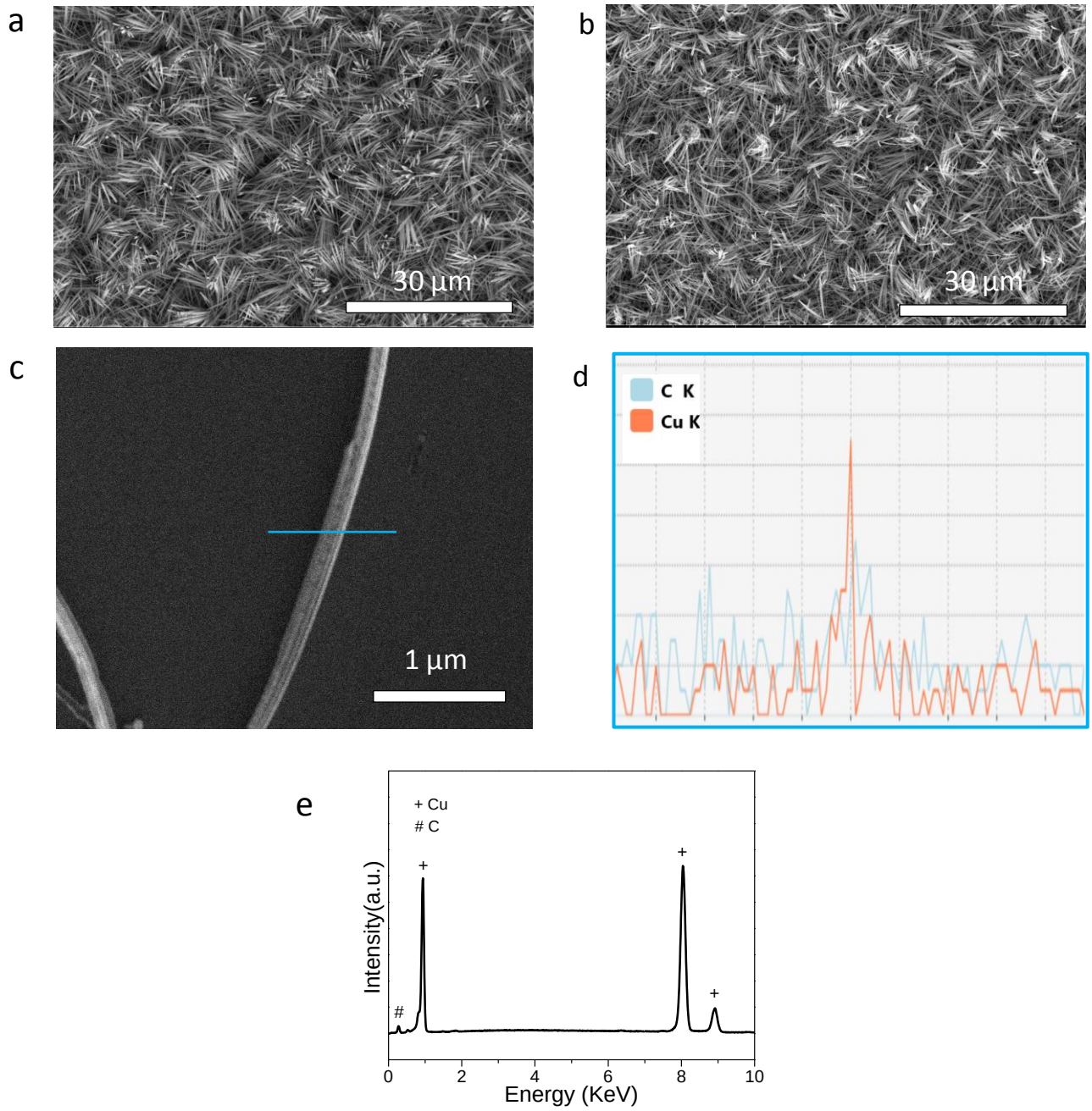

Figure S9. (a) SEM images of $Cu(OH)_2$@C nanowires. **(b,c)** SEM images, **(d)** EDS line-scan profiles and **(e)** EDS spectrum of 3D Cu@C nanowires.

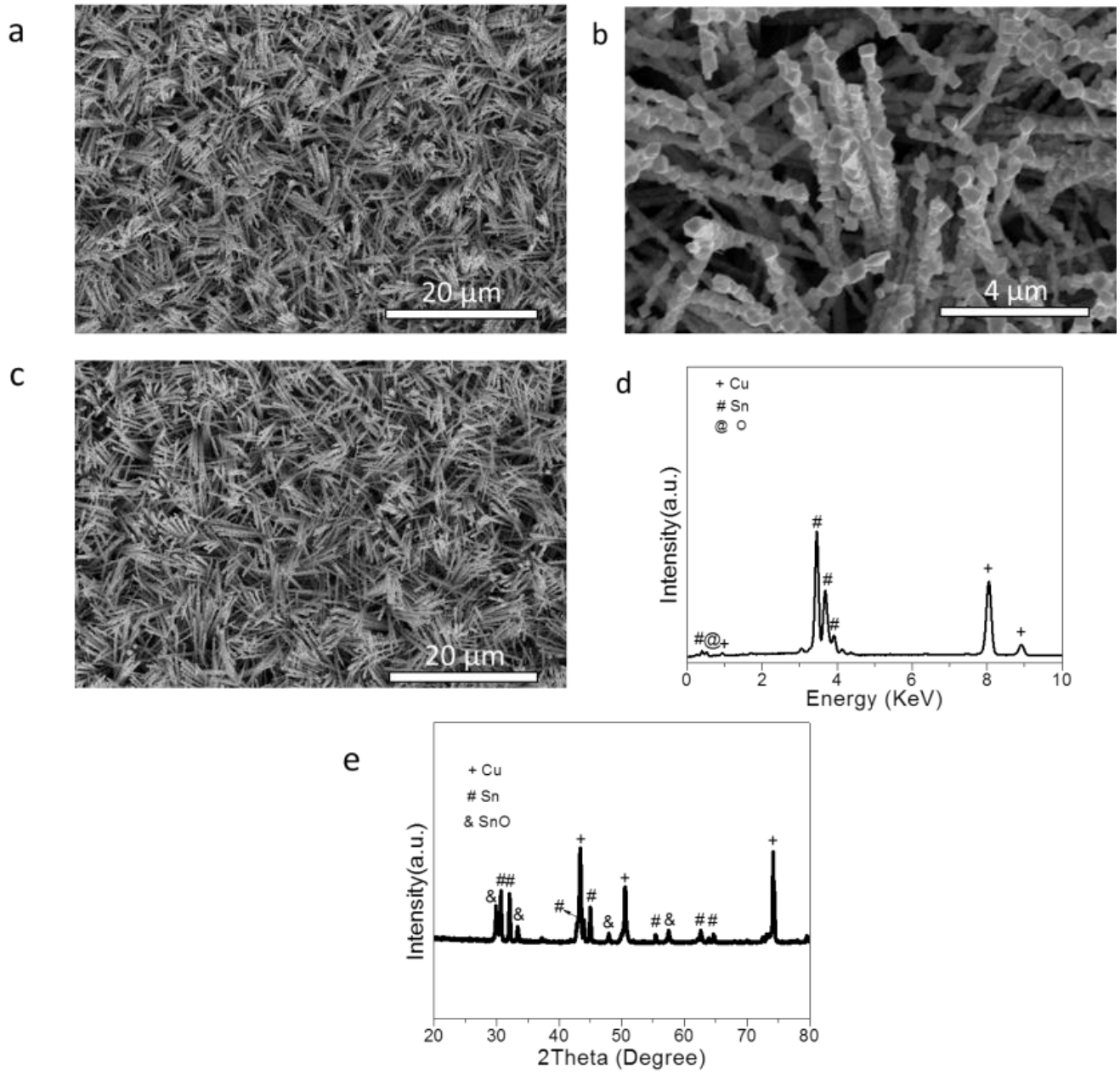

Figure S10. (a,b) SEM images of $Cu(OH)_2$@Sn nanowires. **(c)** SEM image, **(d)** EDS analysis, and **(e)** XRD pattern of 3D Cu@Sn/SnO nanowires.

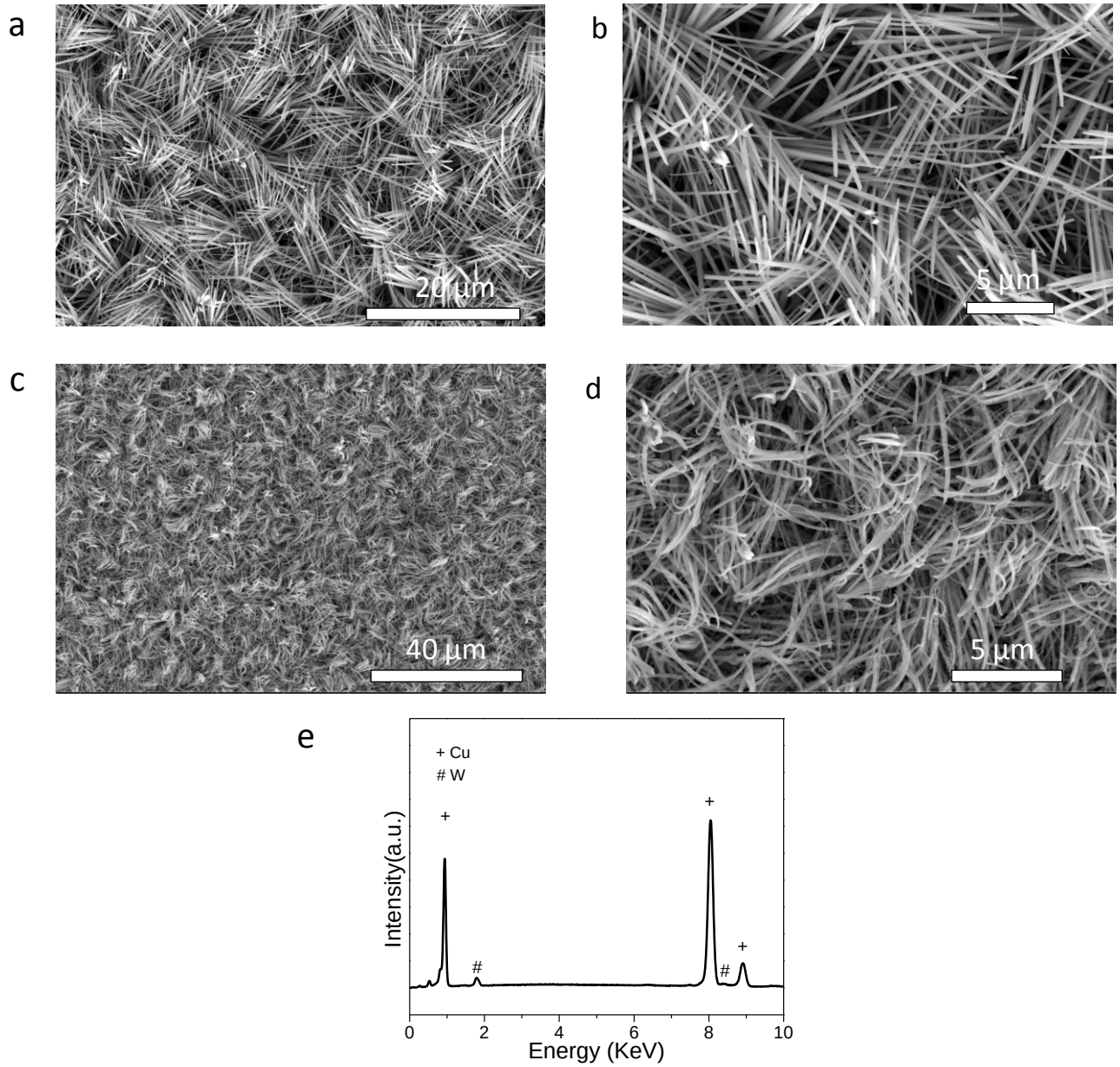

Figure S11. (a,b) SEM images of $Cu(OH)_2$@W nanowires. **(c,d)** SEM images and **(e)** EDS analysis of 3D Cu@W nanowires.

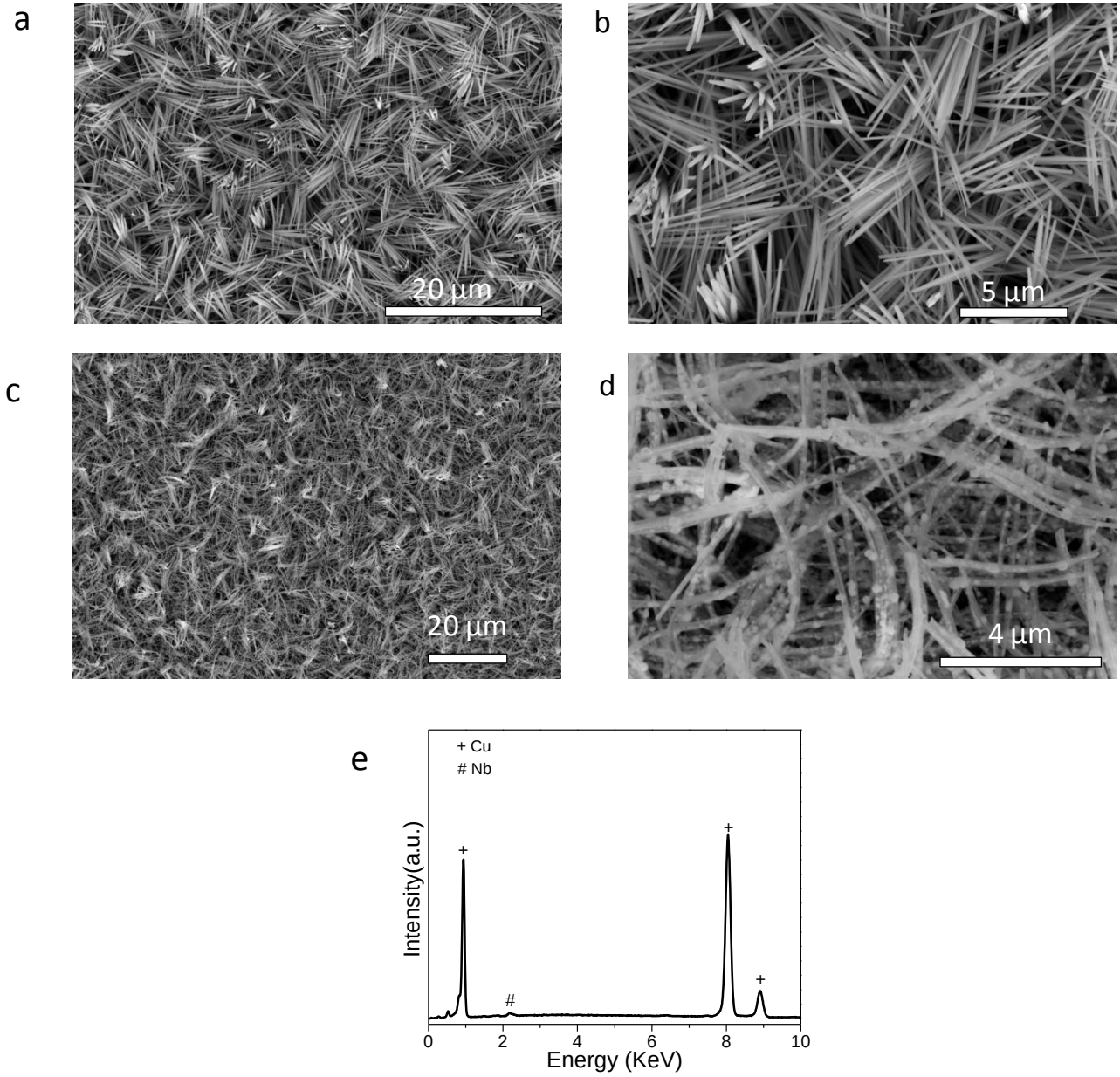

Figure S12. (a,b) SEM images of $Cu(OH)_2$@Nb nanowires. **(c,d)** SEM images and **(e)** EDS analysis of 3D Cu@Nb nanowires.

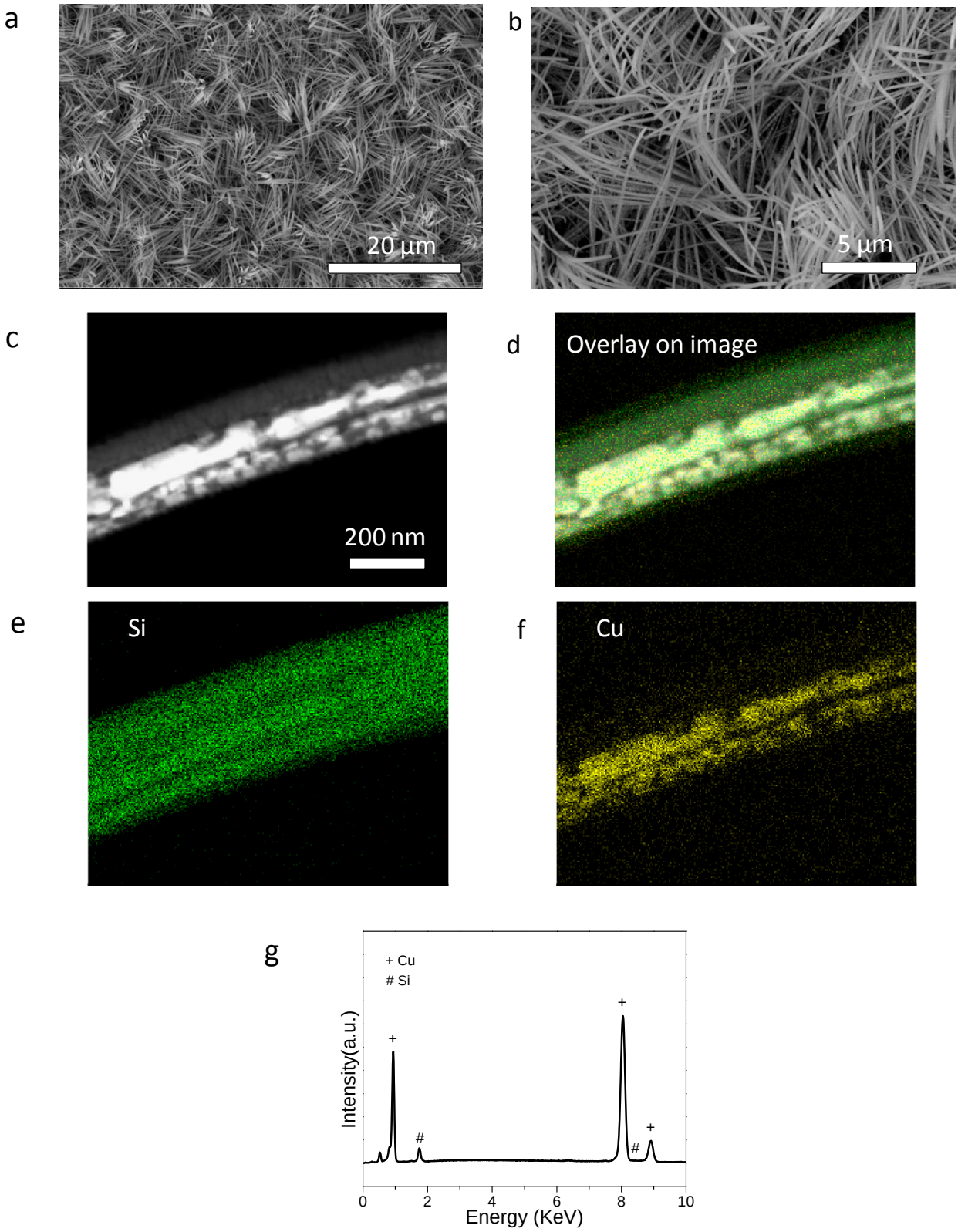

Figure S13. (a) SEM images of $Cu(OH)_2$@Si nanowires. **(b)** SEM image, **(c-f)** HAADF image and the corresponding elements mapping images, and **(g)** EDS spectrum of 3D Cu@Si nanowires.

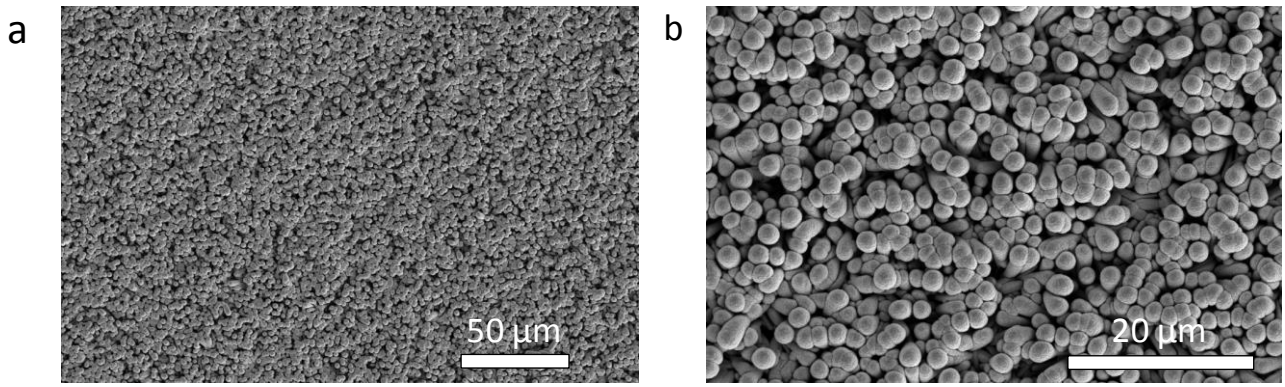

Figure S14. (a,b) SEM images of 3D Cu@Si@Cu nanowires.

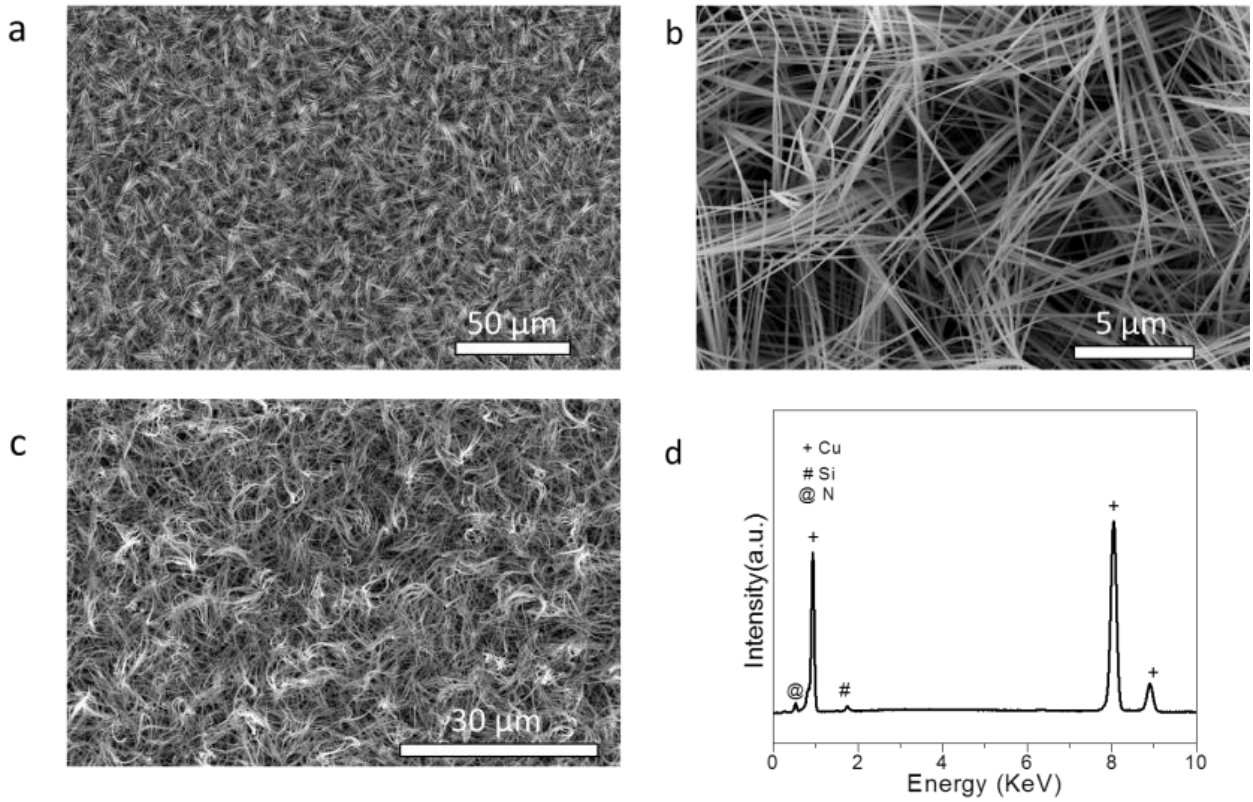

Figure S15. (a,b) SEM images of $Cu(OH)_2$@Si_3N_4 nanowires. **(c)** SEM image and **(d)** EDS spectrum of 3D Cu@Si_3N_4 nanowires.

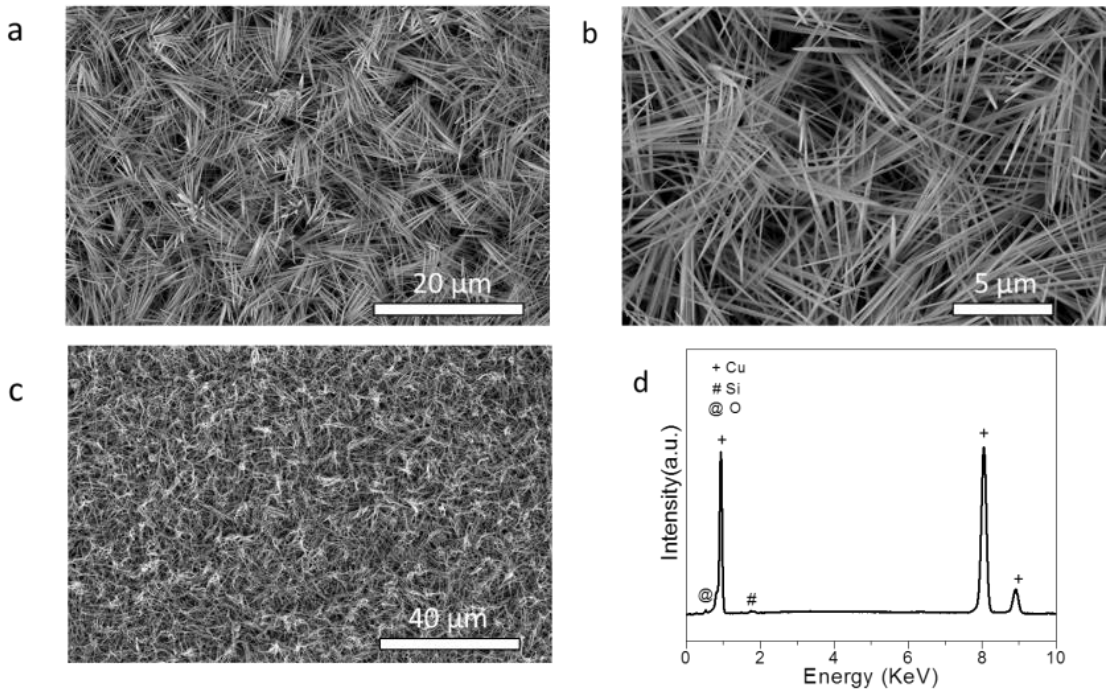

Figure S16. (a,b) SEM images of $Cu(OH)_2$@SiO_2 nanowires. **(c)** SEM image and **(d)** EDS spectrum of 3D Cu@SiO_2 nanowires.

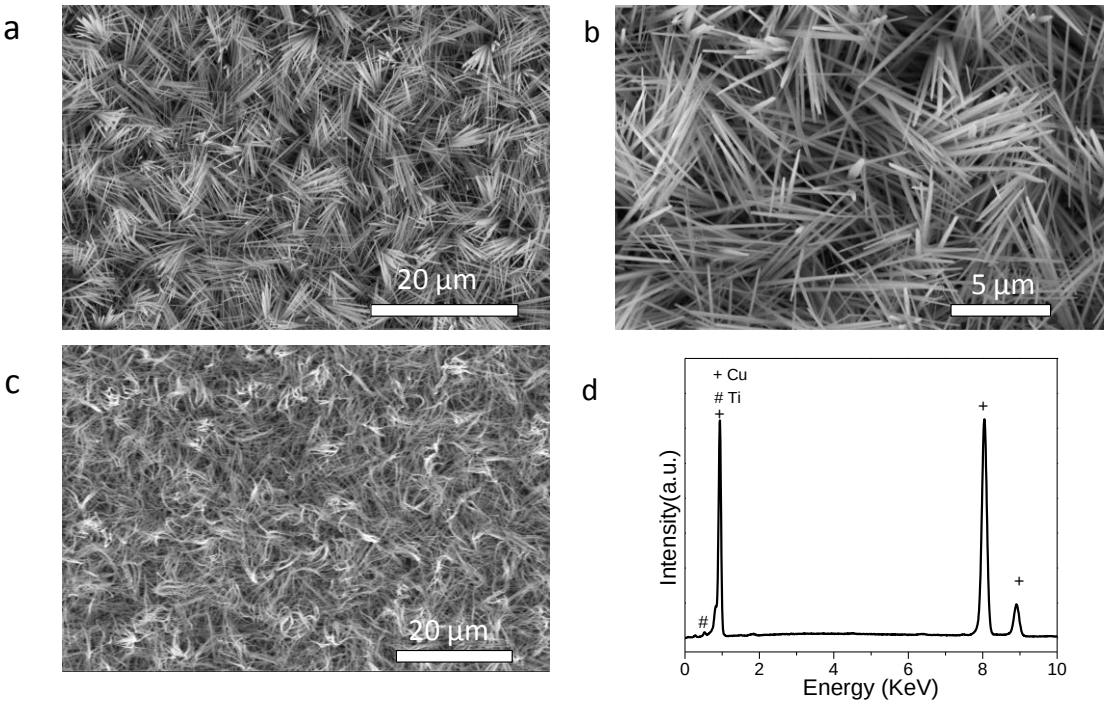

Figure S17. (a,b) SEM images of $Cu(OH)_2$@Ti nanowires. **(c)** SEM image and **(d)** EDS spectrum of 3D Cu@Ti nanowires.

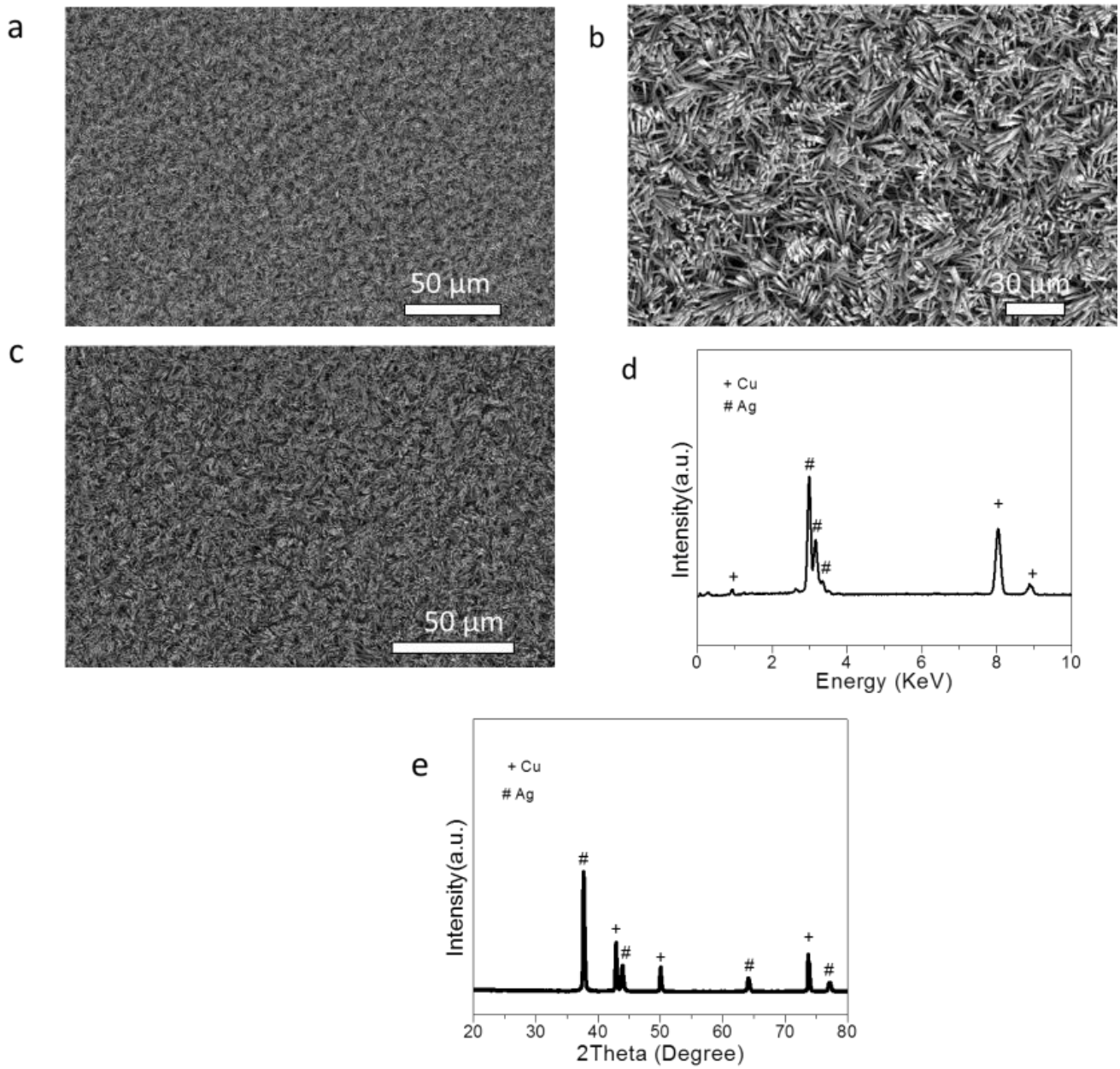

Figure S18. (a,b) SEM images of $Cu(OH)_2$@Ag nanowires. **(c)** SEM image, **(d)** EDS spectrum, and **(e)** XRD pattern of 3D Cu@Ag nanowires.

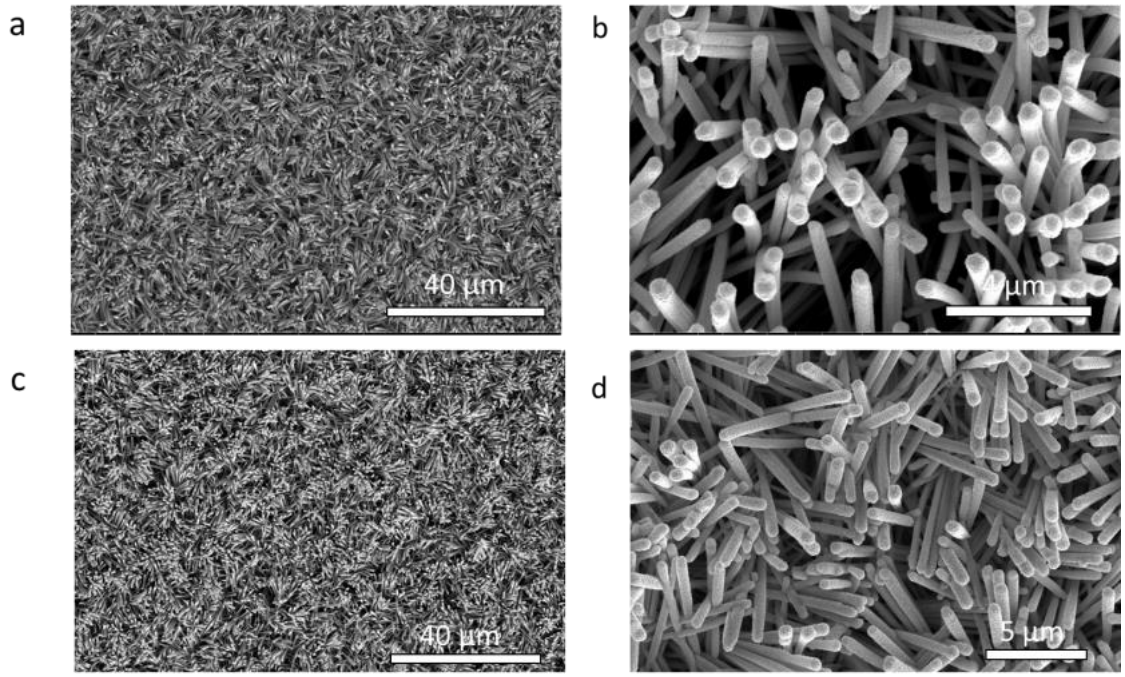

Figure S19. (a,b) SEM images of $Cu(OH)_2$@Fe nanowires. **(c,d)** SEM images of 3D Cu@Fe nanowires.

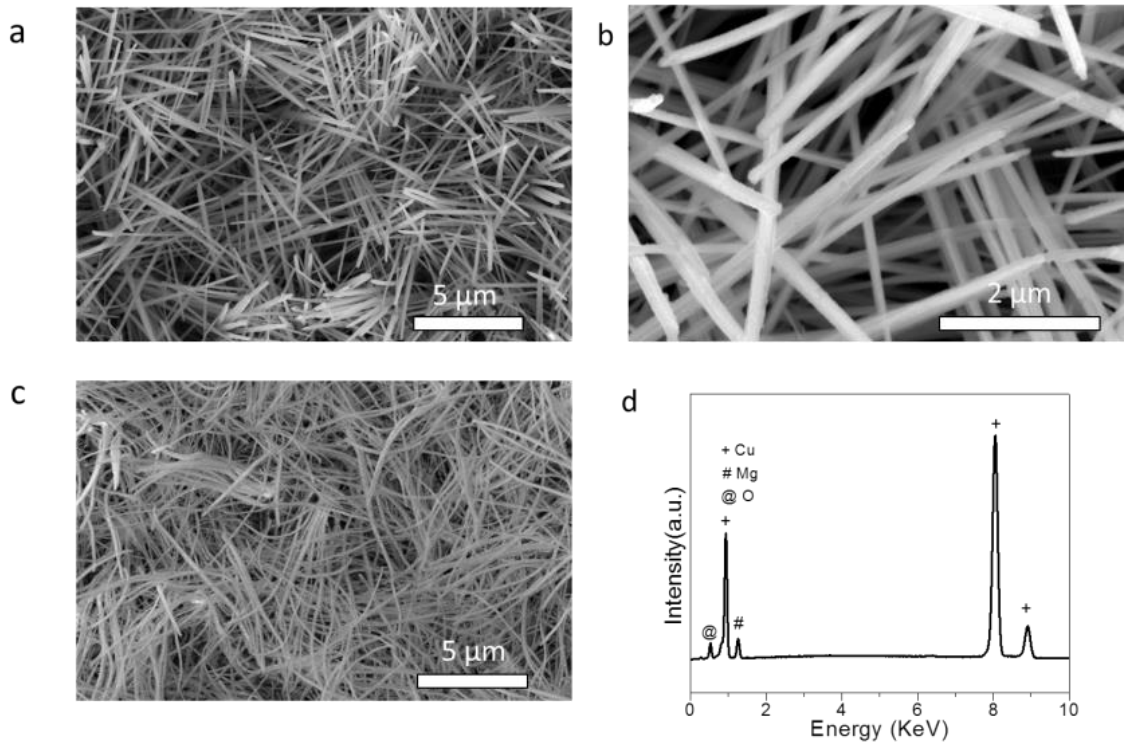

Figure S20. (a,b) SEM images of $Cu(OH)_2$@Mg nanowires. **(c)** SEM images and **(d)** EDS spectrum of 3D Cu@MgO nanowires.

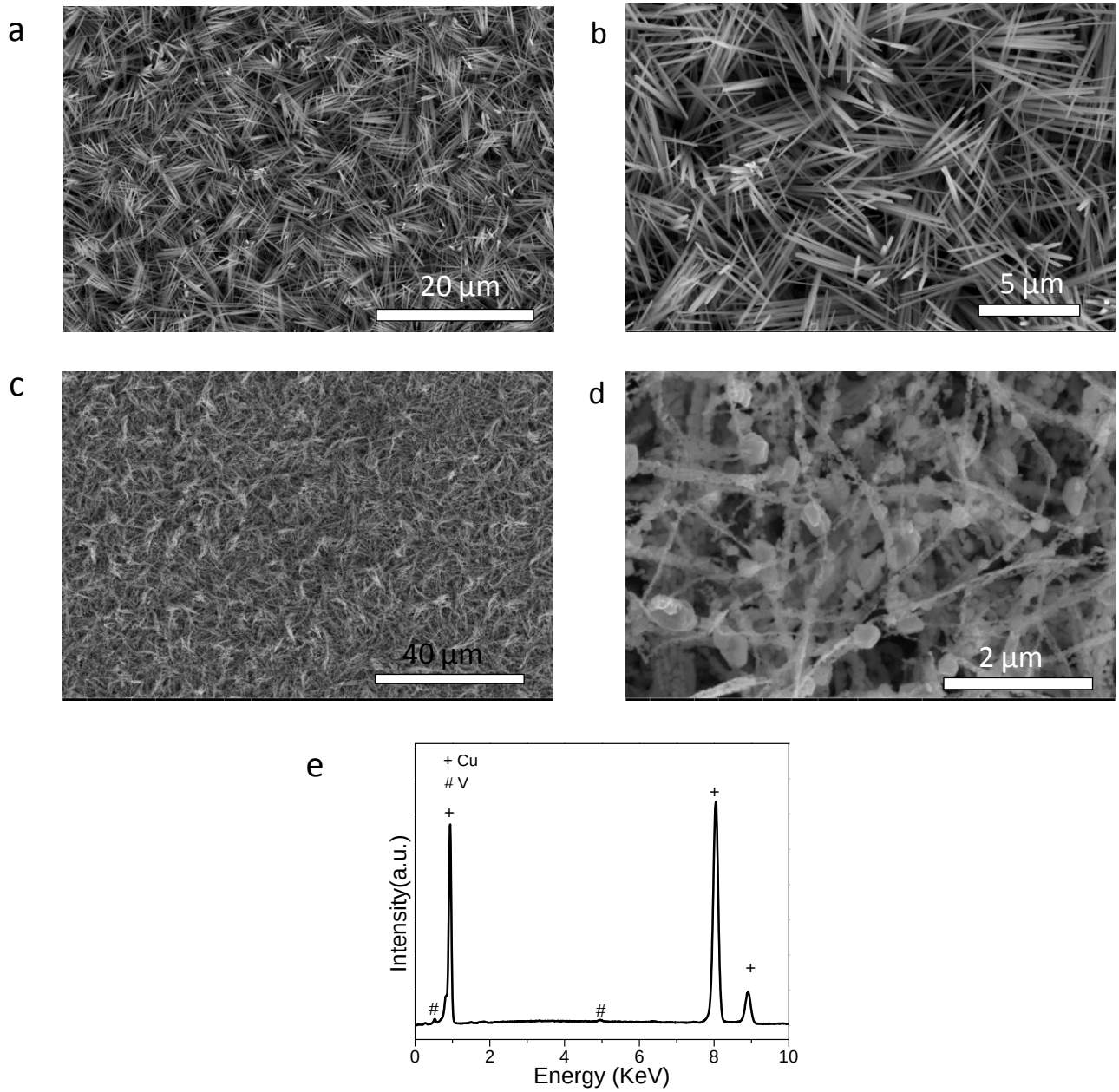

Figure S21. (a,b) SEM images of $Cu(OH)_2$@V nanowires. **(c,d)** SEM images, and **(e)** EDS spectrum of 3D Cu@V nanowires.

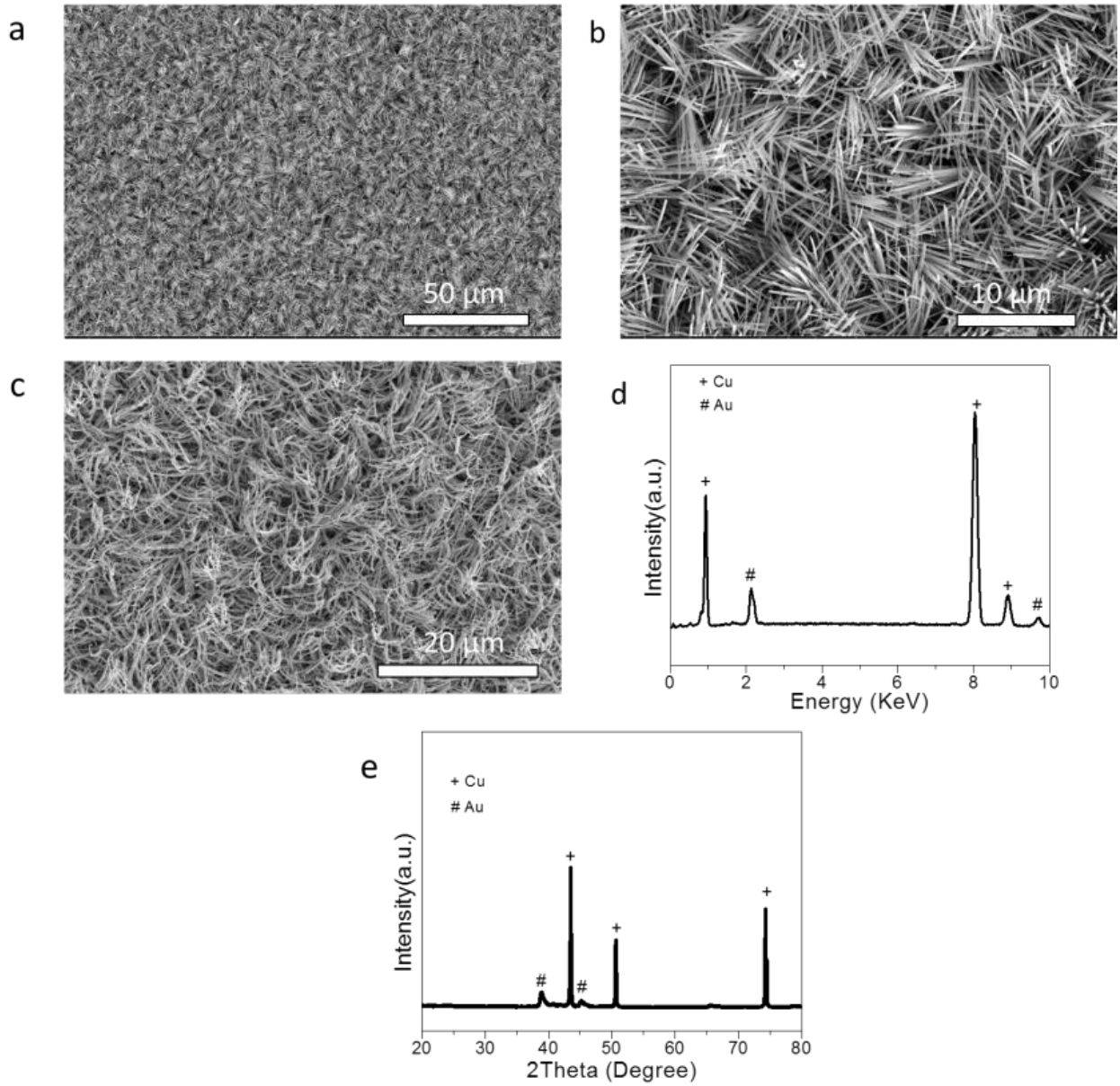

Figure S22. (a,b) SEM images of $Cu(OH)_2$@Au nanowires. **(c)** SEM image, **(d)** EDS spectrum, and **(e)** XRD pattern of 3D Cu@Au nanowires.

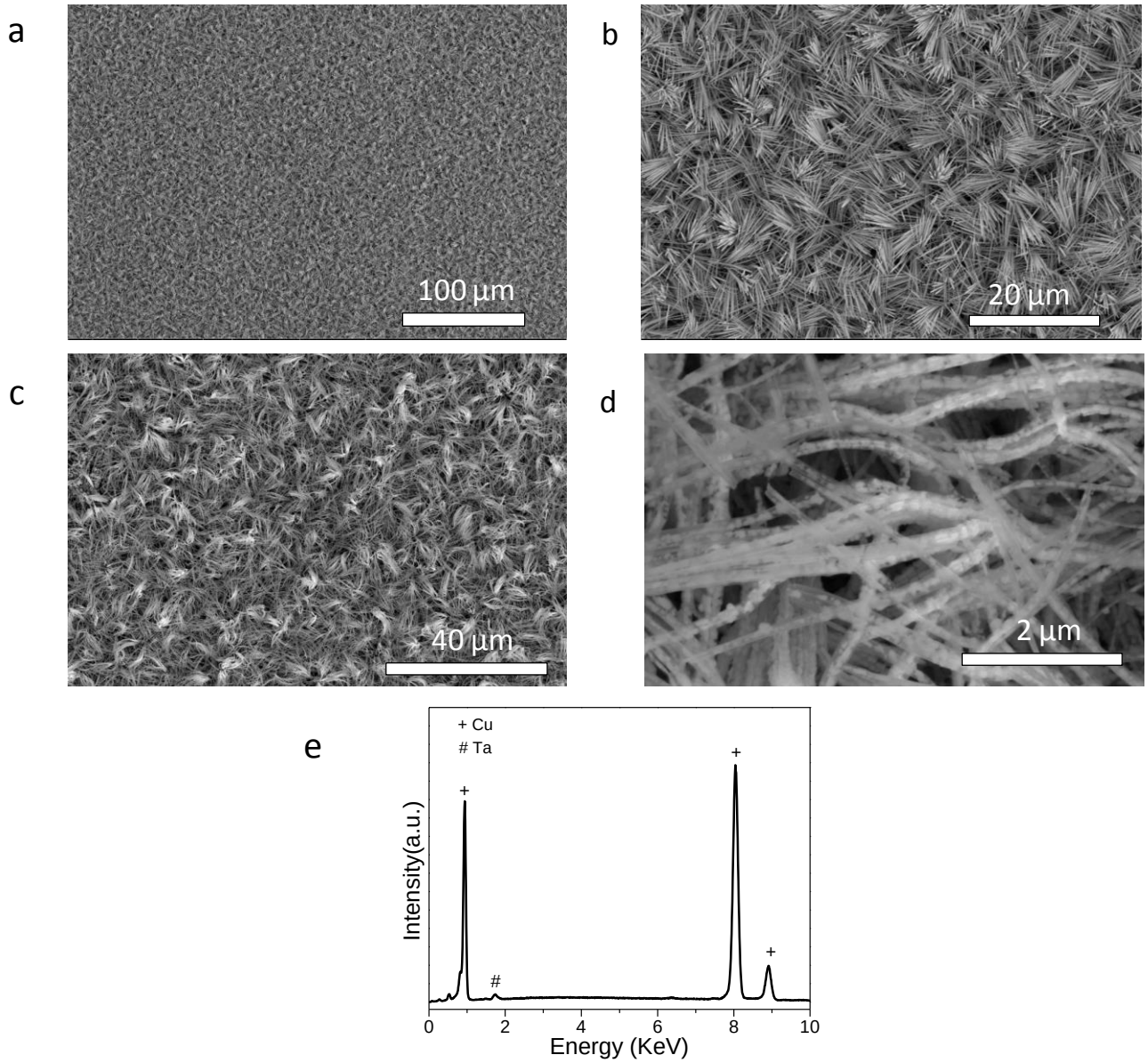

Figure S23. (a,b) SEM images of $Cu(OH)_2$@Ta nanowires. **(c,d)** SEM images and **(e)** EDS spectrum of 3D Cu@Ta nanowires.

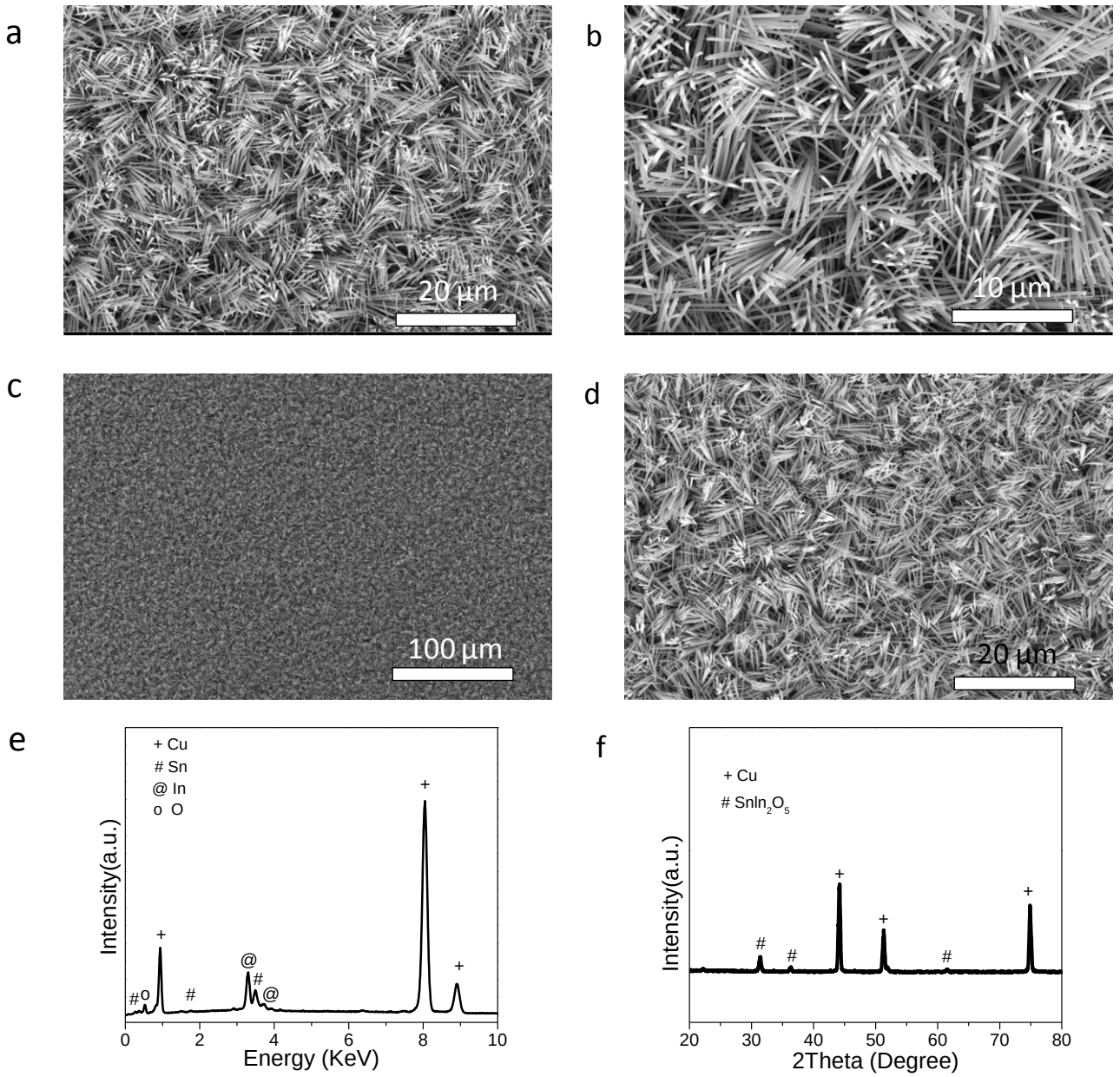

Figure S24. (a,b) SEM images of $Cu(OH)_2$@$SnIn_2O_5$ nanowires. **(c,d)** SEM images, **(e)** EDS spectrum, and **(f)** XRD pattern of 3D Cu@$SnIn_2O_5$ nanowires.

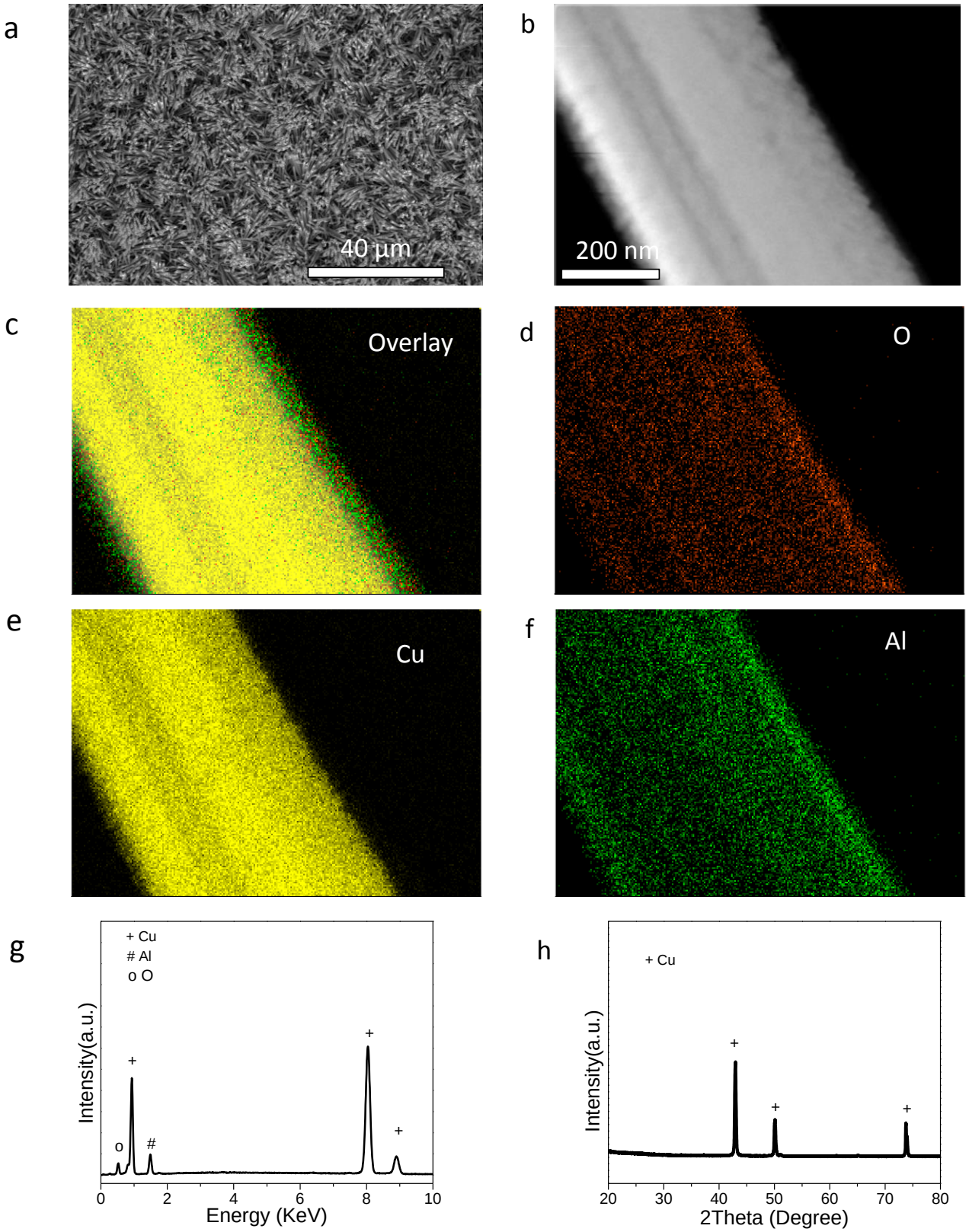

Figure S25. (a) SEM image, **(b)** HAADF image, **(c-f)** the corresponding elemental mappings, **(g)** EDS spectrum and **(h)** XRD pattern of 3D Cu@Al_2O_3 nanowires.

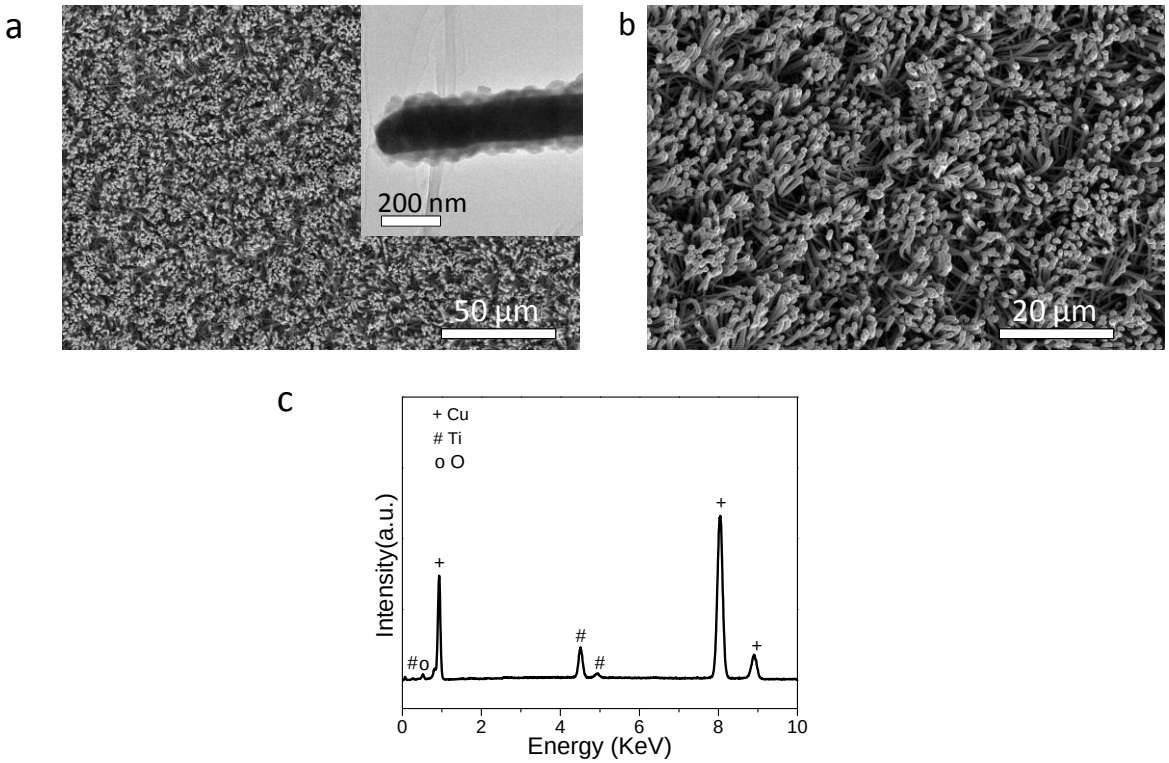

Figure S26. (a,b) SEM images (the inset is a TEM image) and **(c)** EDS spectrum of 3D Cu@TiO_2 nanowires.

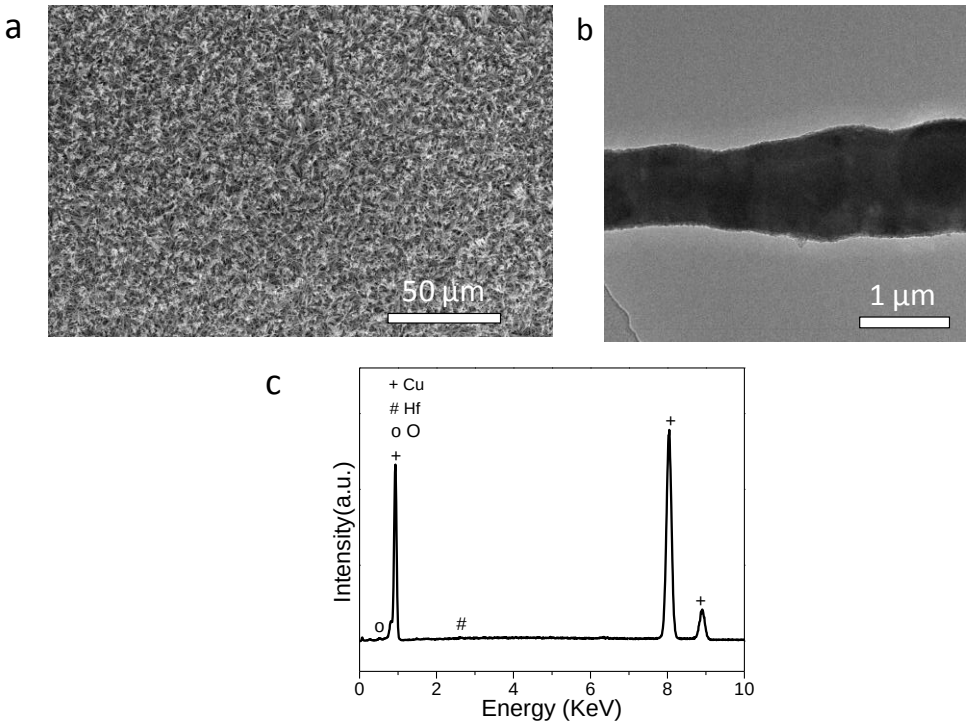

Figure S27. (a) SEM image, **(b)** TEM image, and **(c)** EDS spectrum of 3D Cu@HfO_2 nanowires.

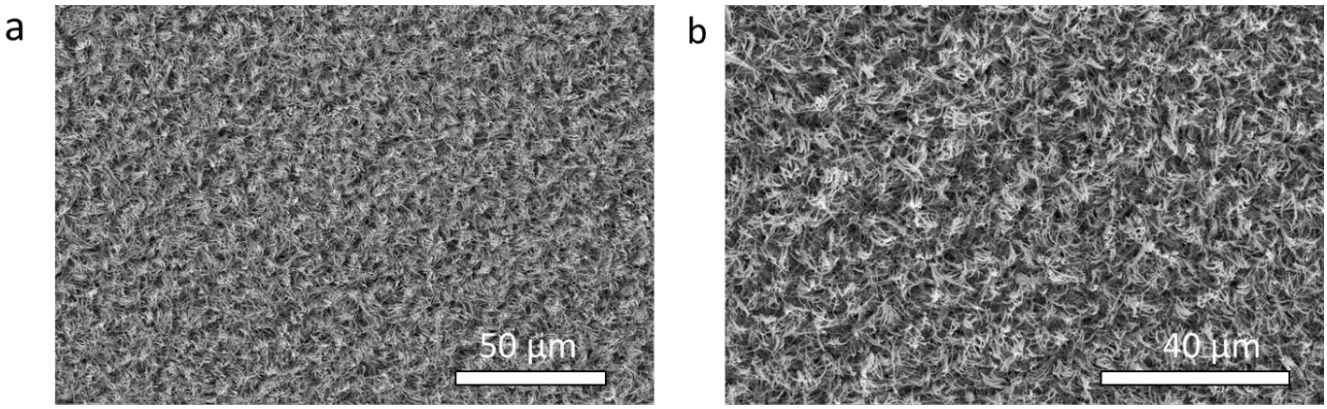

Figure S28. SEM images of **(a)** $Cu(OH)_2$@Au nanowires on Cu foil prepared by thermal evaporation. **(b)** 3D Cu@Au nanowires by H_2-reduction.

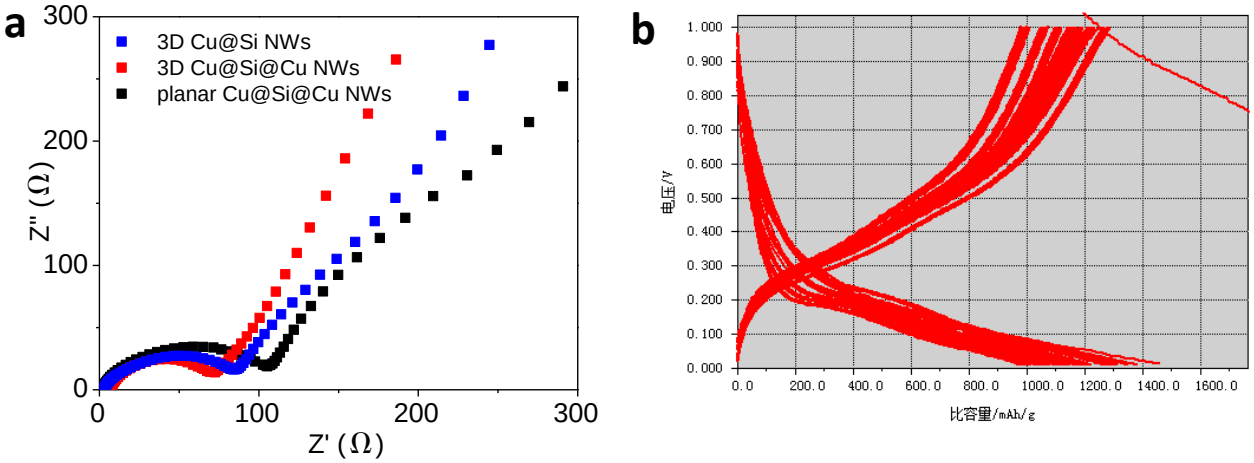

Figure S29. (a) Impedance measurements of 3D Cu@Si, 3D Cu@Si@Cu NWs and planar Cu@Si@Cu NWs after 1500 cycles. **(b)** Galvanostatic discharge/charge profiles at different rates from 1C to 10C for 3D Cu@Si@Cu NWs in half-cell configuration.

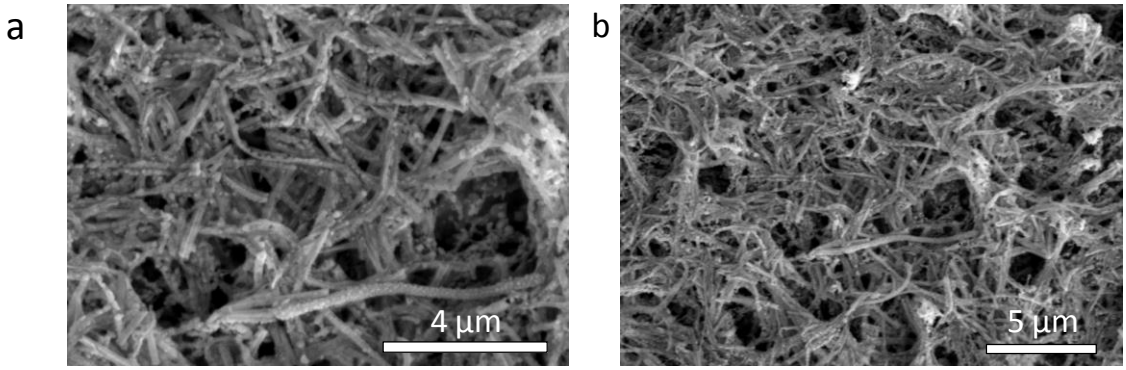

Figure S30. (a,b) SEM images of 3D Cu@Si nanowires electrode after 2000 cycles, etched with HCl and H_2 reduction at 400 ^{o}C.

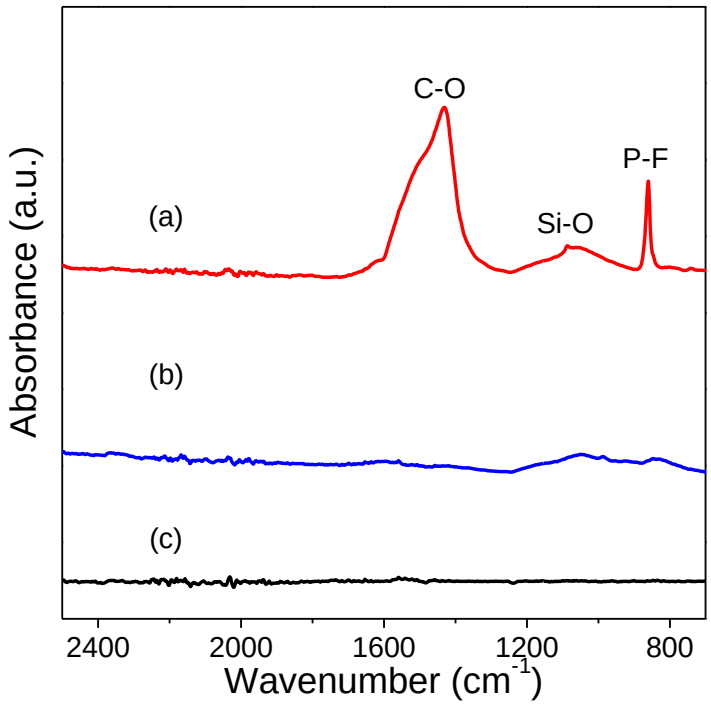

Figure S31. FTIR spectra of 3D Cu@Si electrodes (a) after cycling test, (b) etched by HCl after cycling test, and (c) further reduced with H_2 after etching.

Compared with 3D Cu@Si electrodes after cycling test, the FTIR spectra for the sample after etching SEI with HCl and further H_2-reduction showed dimished F-P, C-O, Si-O stretching bands, indicating removal of most of these surface groups from the SEI after post treatment.[2-4]

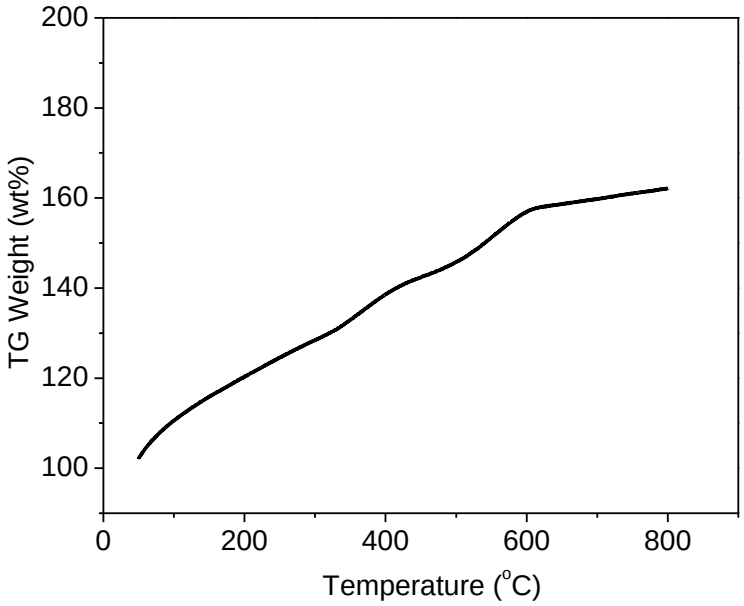

Figure S32. TG analysis of 3D Cu@Si nanowires in air at a heating rate of 10 ^{o}C min^{-1}.

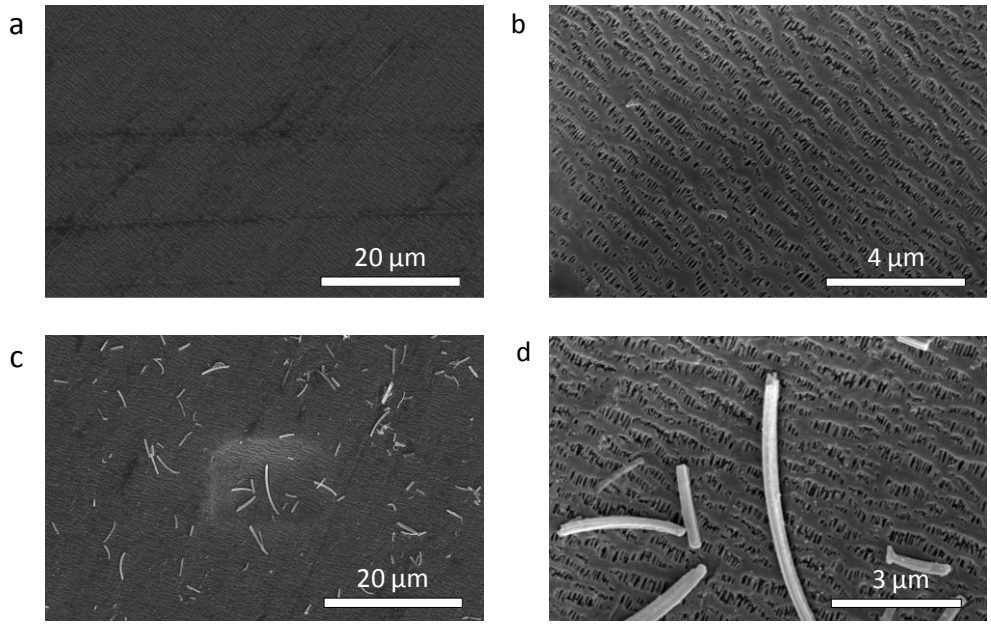

Figure S33. SEM images of polypropylene microporous separator **(a,b)** before and **(c,d)** after battery cycling test.

After cycling test, the porous structure of polypropylene microporous films was well maintained.

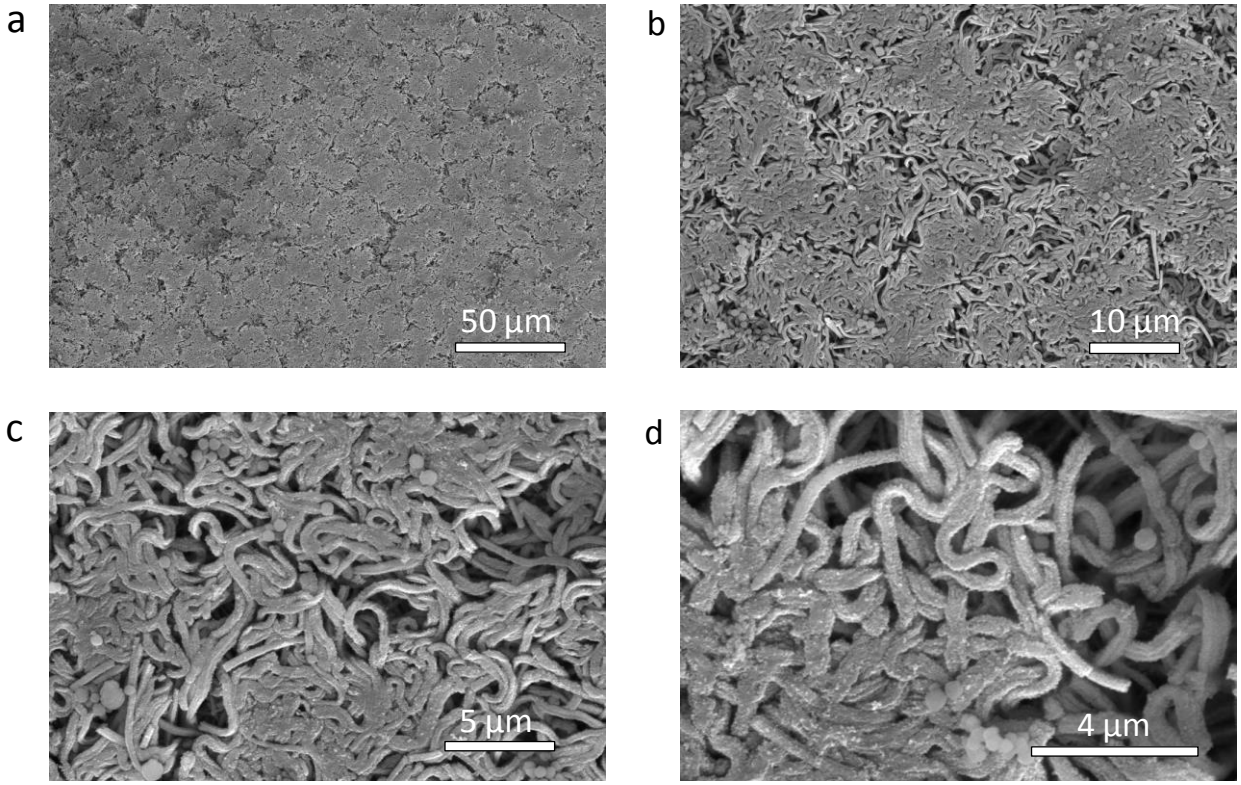

Figure S34. SEM images of 3D Cu@Si@Cu nanowires after 12000 cycles in half-cell configuration.

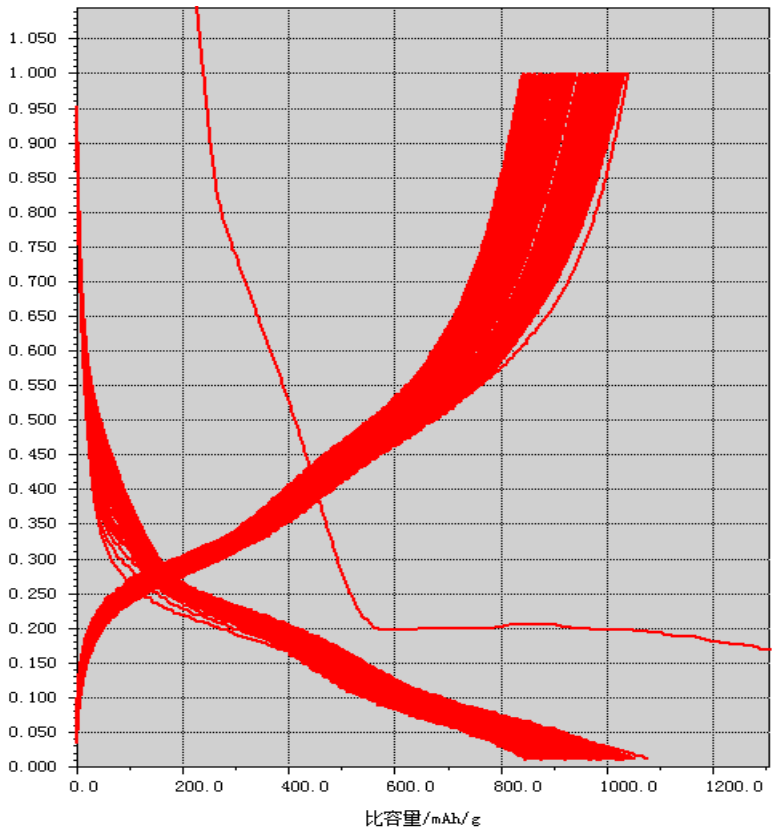

Figure S35. Electrochemical test raw data of 3D Cu@Si@Cu microparticles at a Si loading of 1.08 mg/cm^2 in half-cell configuration.

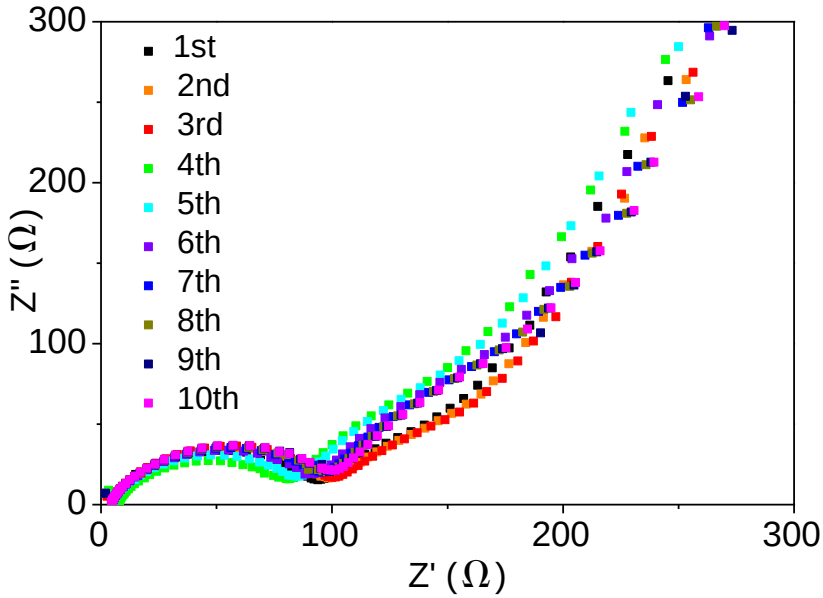

Figure S36. Impedance measurements of 3D Cu@Si@Cu microparticles for the first 10 cycles.

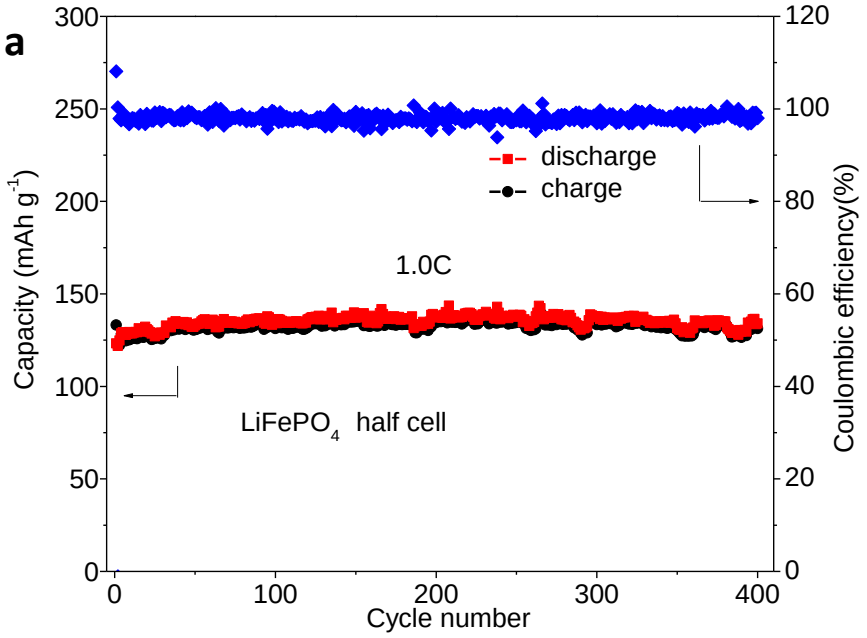

Figure S37. Cycling performance and coulombic efficiency of $LiFePO_4$ at 1C for 400 cycles.

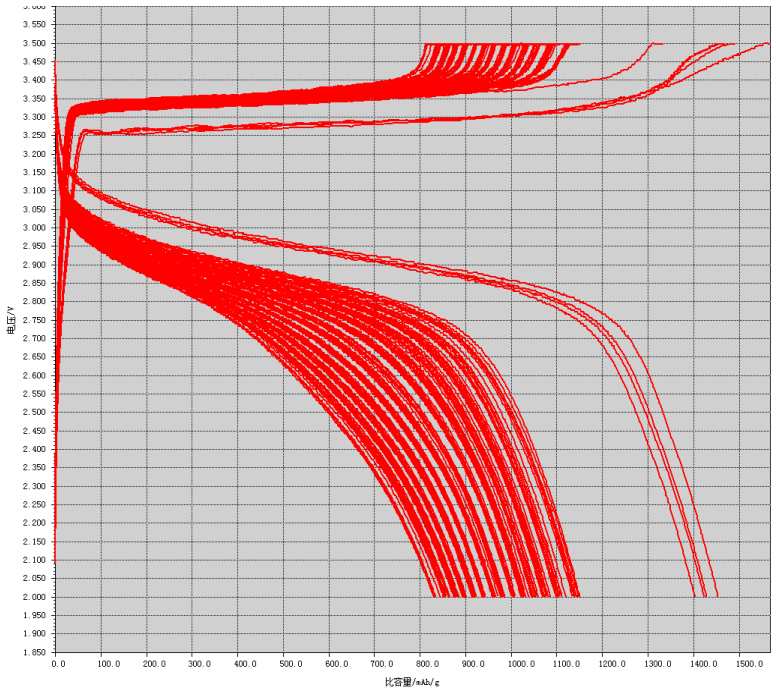

Figure S38. Electrochemical test raw data of 3D Cu@Si@Cu-$LiFePO_4$ full cell (Si loading 1.08 mg/cm^2).

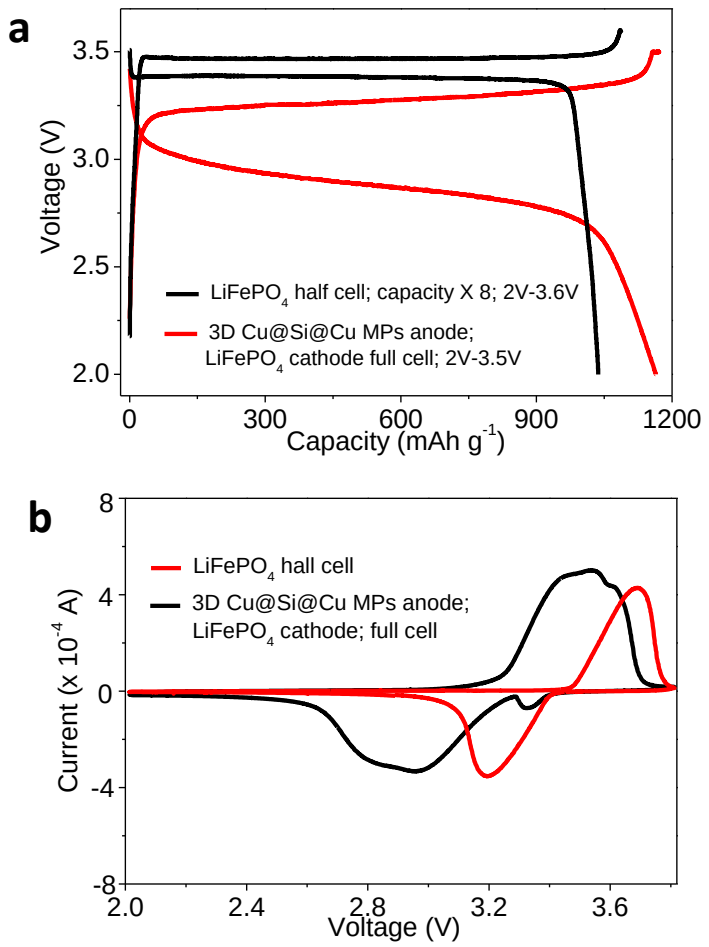

Figure S39. (a) The voltage profiles and **(b)** CV curves of 3D Cu@Si@Cu-$LiFePO_4$ full cells and Li-$LiFePO_4$ half cells. The capacity and rate are both based on the mass loading of Si in the anode.

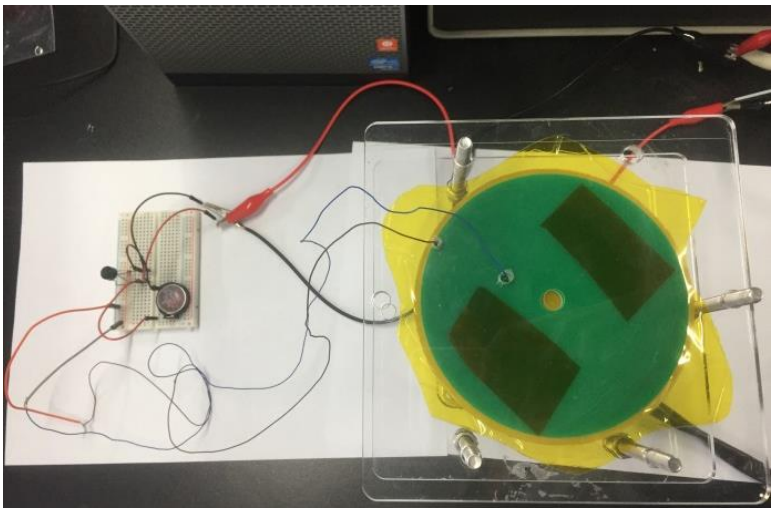

Figure S40. The photograph of battery charging test by a TENG with the aid of a Zener diode and a rectifier.

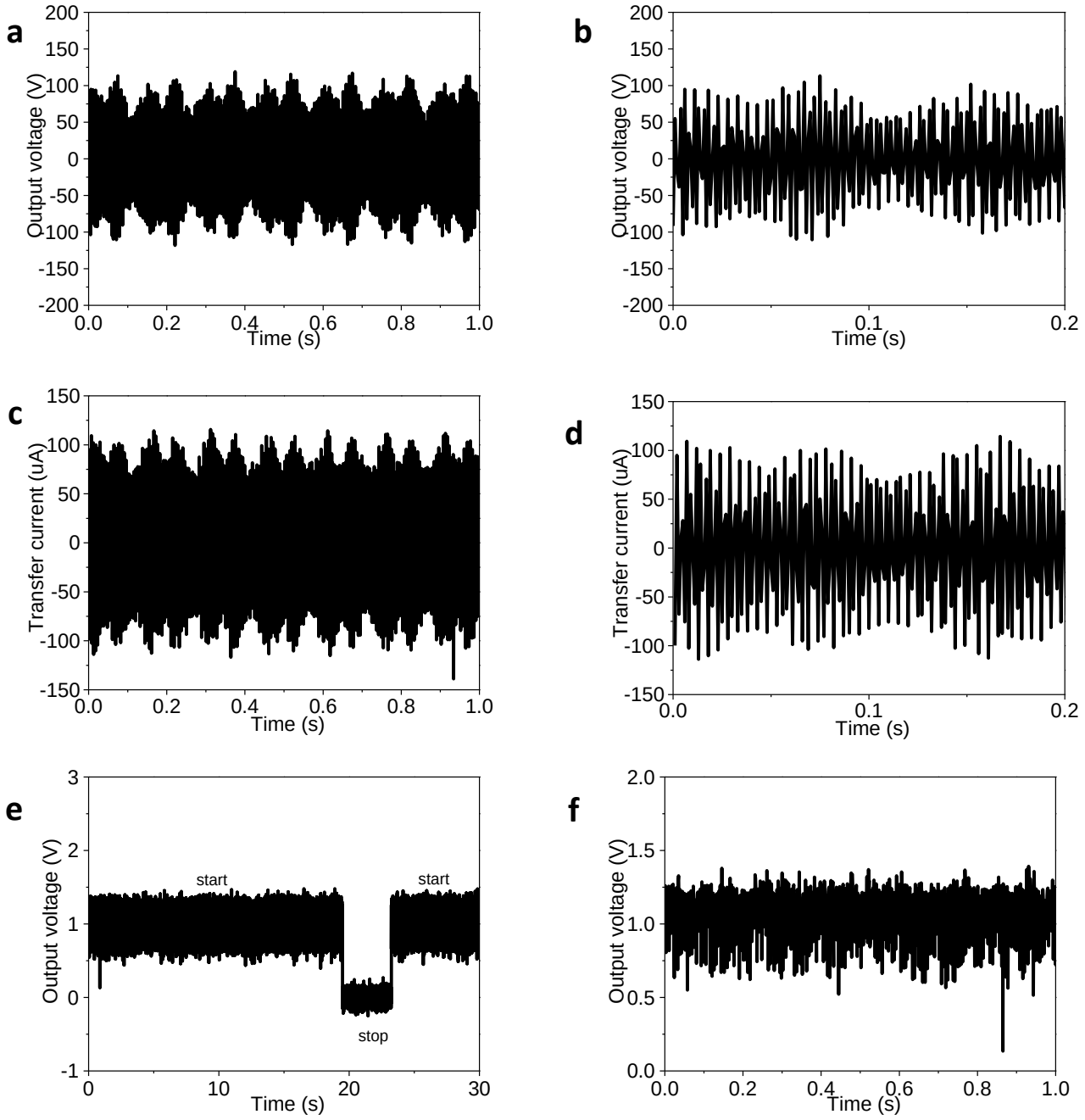

Figure S41. Voltage and current of a rotating TENG for 3D Cu@Si@Cu half-cell charging**. (a,b)** Open-circuit voltage at 350 rpm. **(c,d)** Short-circuit current. **(e,f)** Open-circuit voltage of the TENG connected to a Zener diode and a rectifier. The voltage and current were measured at an air humidity of 23%-36%.

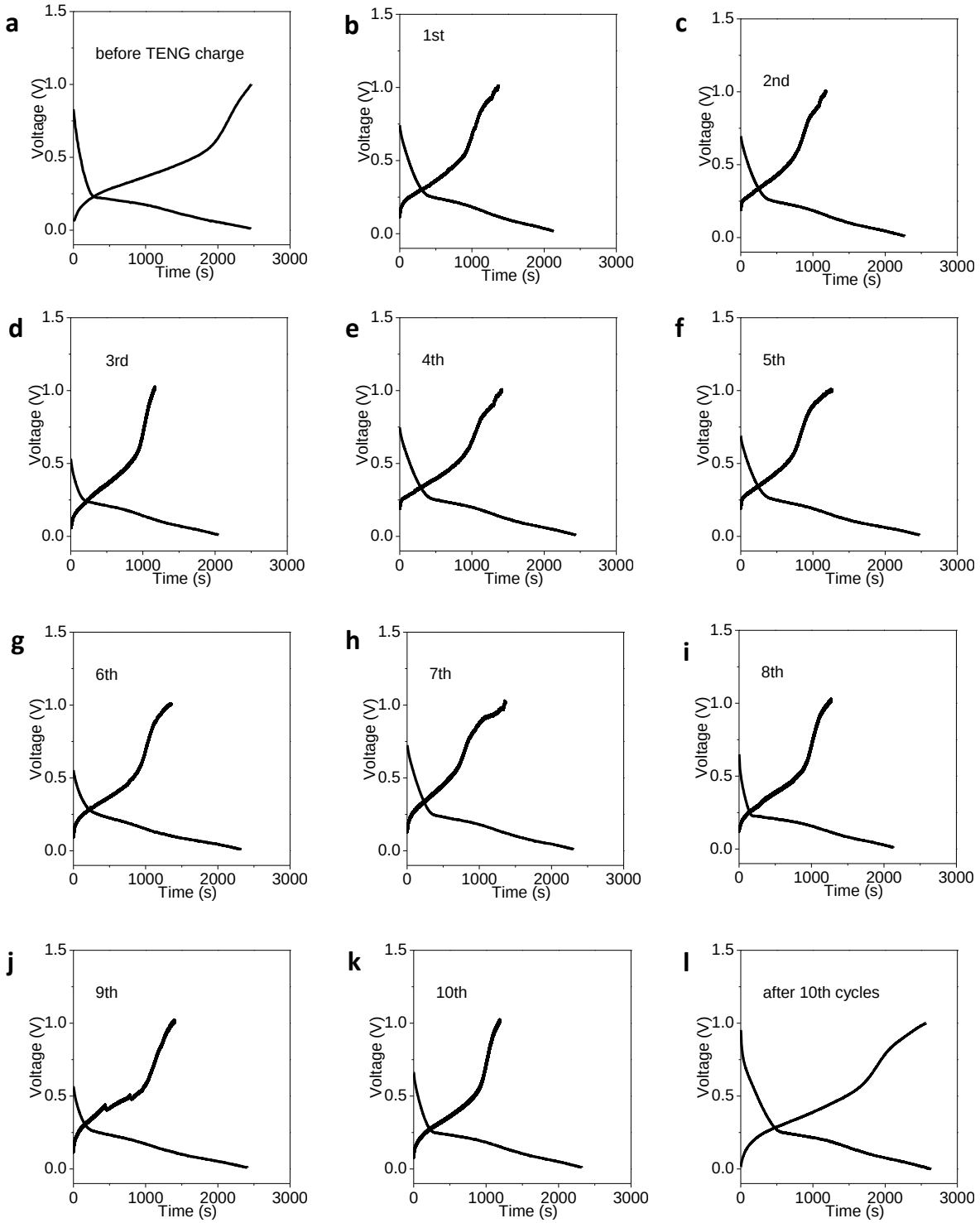

Figure S42. Discharge/charge profiles of 3D Cu@Si@Cu in half-cell configuration. **(a)** Charged and discharged at constant currents. (**b-k)** Charged by TENG and discharged at a constant current. **(l)** Charged and discharged at constant currents after 10 cycles of TENG charging and constant current discharging.

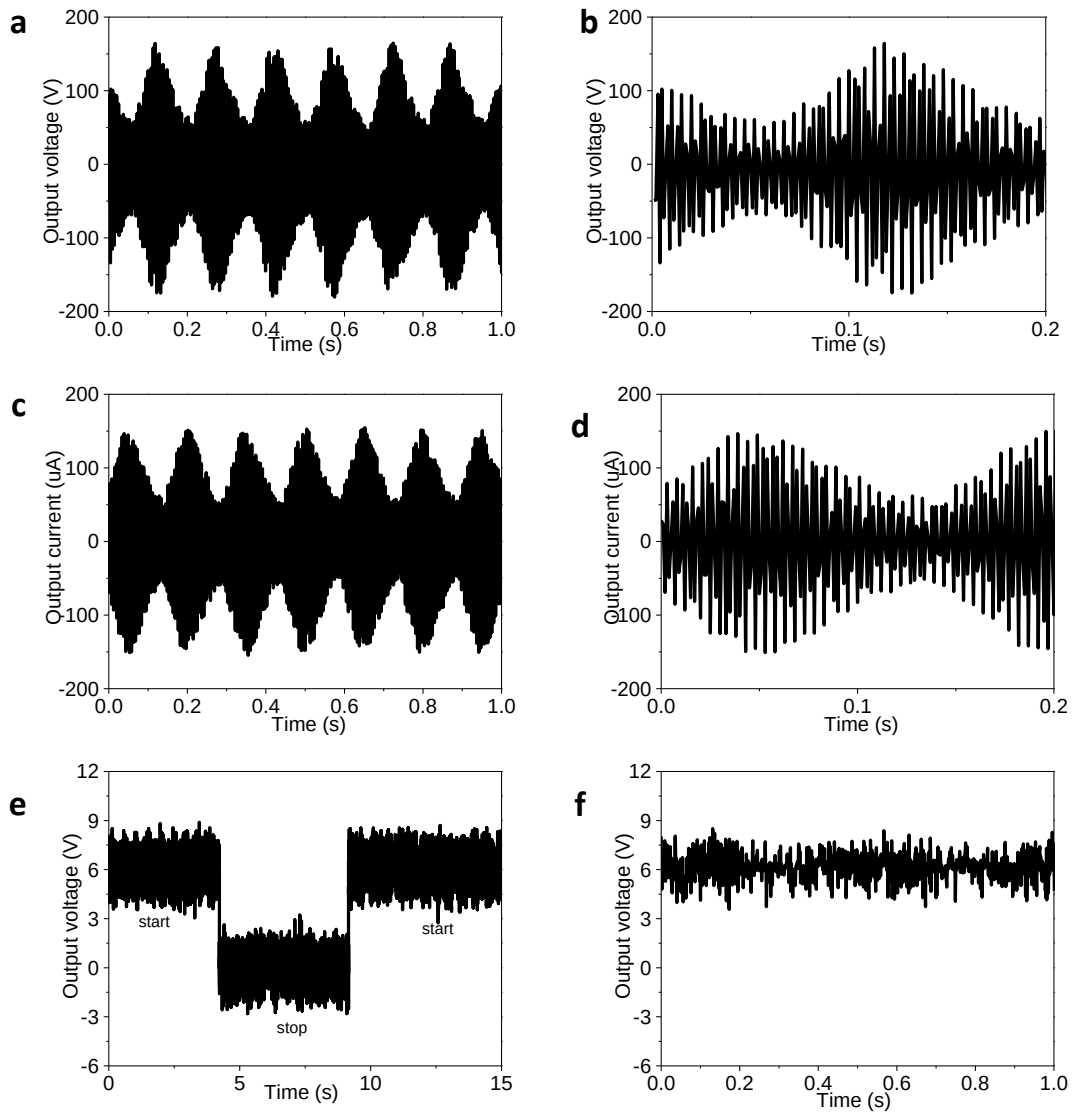

Figure S43. Voltage and current of a rotating TENG for 3D Cu@Si@Cu-$LiFePO_4$ full-cell charging. **(a,b)** Open-circuit voltage at 400 rpm. **(c,d)** Short-circuit current. **(e,f)** Open-circuit voltage of the TENG connected to a Zener diode and a rectifier. Air humidity: 18%-25%.

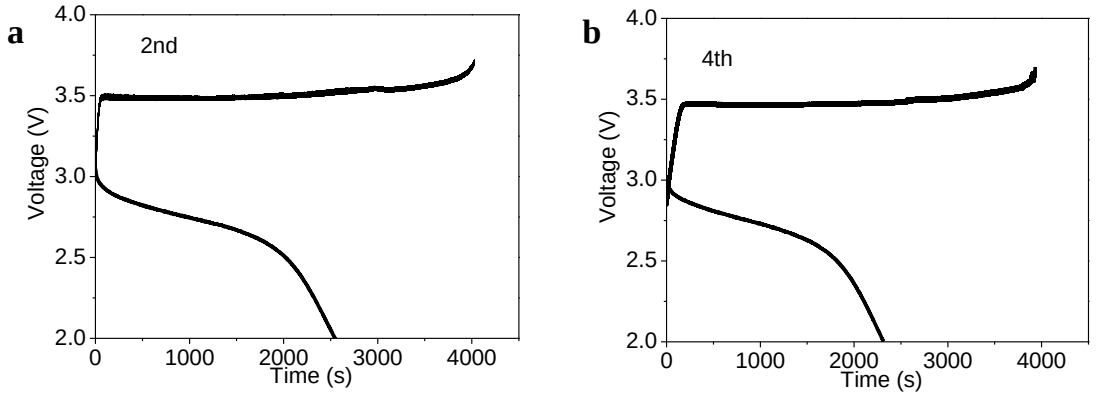

Figure S44. A 3D Cu@Si@Cu-$LiFePO_4$ full cell charged by TENG and discharged at a constant current for **(a)** the 2nd and **(b)** the 4th cycles.

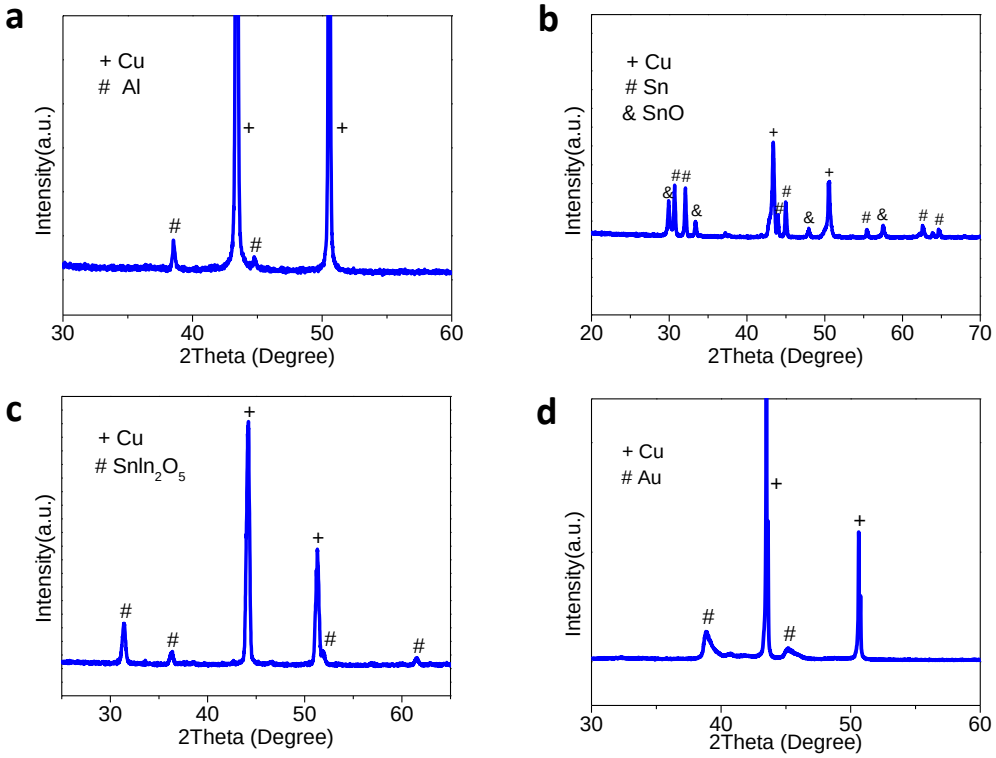

Figure S45. XRD patterns of **(a)** 3D Cu@Al NWs, **(b)** 3D Cu@Sn/SnO NWs, **(c)** 3D Cu@$SnIn_2O_5$ NWs, and **(d)** 3D Cu@Au NWs.

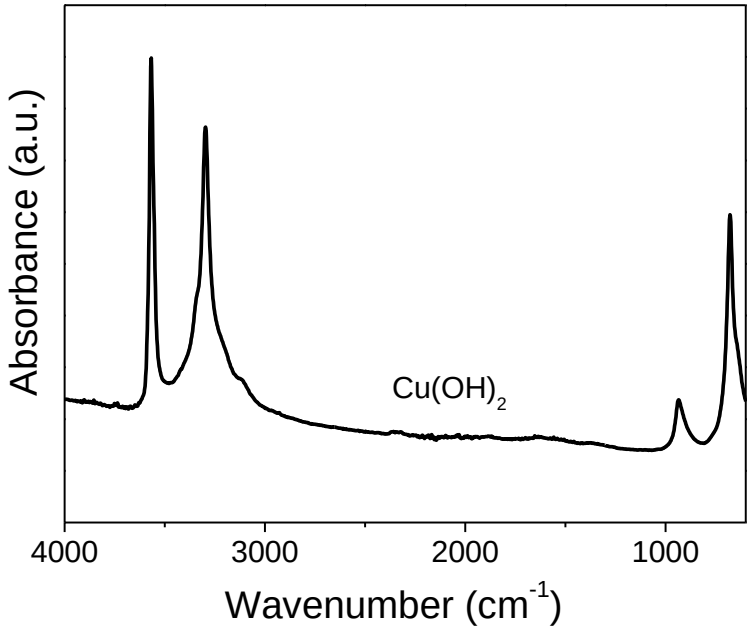

Figure S46. FTIR spectra of $Cu(OH)_2$ nanowires. The FTIR spectra indicated the surface of $Cu(OH)_2$ nanowires is rich of -OH groups.

Table S1. The power and duration of magnetron sputtering for the deposition of Cu, Al, C, Si, SiO_2, Si_3N_4, Ag, Ti, Ta, W, $SnIn_2O_5$, Au, V, Nb, Mg, Fe, Ni, Sn, ZnO, TiN on $Cu(OH)_2$ nanowires.

Samples	power (W)	duration (h)
$Cu(OH)_2$@Cu	100	1
$Cu(OH)_2$@Al	100	0.5
$Cu(OH)_2$@C	300	0.5
$Cu(OH)_2$@Si	300	1
$Cu(OH)_2$@SiO_2	100	0.5
$Cu(OH)_2$@Si_3N_4	100	0.5
$Cu(OH)_2$@Ag	100	1
$Cu(OH)_2$@Ti	50	0.5
$Cu(OH)_2$@Ta	100	1
$Cu(OH)_2$@W	100	1
$Cu(OH)_2$@$SnIn_2O_5$	100	1
$Cu(OH)_2$@Au	50	1
$Cu(OH)_2$@V	50	1
$Cu(OH)_2$@Nb	100	0.5
$Cu(OH)_2$@Mg	50	0.5
$Cu(OH)_2$@Fe	100	1
$Cu(OH)_2$@Ni	100	1
$Cu(OH)_2$@Sn	50	0.5
$Cu(OH)_2$@ZnO	100	1
$Cu(OH)_2$@TiN	100	1

REFERENCES

(1) Zhang, W. X.; Wen, X. G.; Yang, S. H.; Berta, Y.; Wang, Z. L. Single-Crystalline Scroll-Type Nanotube Arrays of Copper Hydroxide Synthesized at Room Temperature. *Adv. Mater.* **2003,** 15, 822-825.

(2) Shi, F. F.; Ross, P. N.; Somorjai, G. A.; Komvopoulos, K. The Chemistry of Electrolyte Reduction on Silicon Electrodes Revealed by *in situ* ATR-FTIR Spectroscopy. *J. Phys. Chem. C* **2017,** 121, 14476-14483.

(3) Singh, S.; Raj, A. K.; Sen, R.; Johari, P.; Mitra, S. Impact of Cl Doping on Electrochemical Performance in Orthosilicate (Li_2FeSiO_4): A Density Functional Theory Supported Experimental Approach. *ACS Appl. Mater. Interfaces* **2017,** 9, 26885-26896.

(4) Karakassides, M. A.; Gournis, D.; Petridis, D. An Infrared Reflectance Study of Si-O Vibrations in Thermally Treated Alkali-Saturated Montmorillonites. *Clay Miner.* **1999,** 34, 429-438.